SSD-TDR-63-261

Surface Impedance of a Thin Plasma Sheet

7 OCTOBER 1963

Prepared by T. M. SMITH and K. E. GOLDEN
Plasma Research Laboratory

Prepared for COMMANDER SPACE SYSTEMS DIVISION
UNITED STATES AIR FORCE
Inglewood, California

LABORATORIES DIVISION • AEROSPACE CORPORAT
CONTRACT NO. AF 04(695)

SSD-TDR-63-261

Report No.
TDR-269(4280-10)-1

SURFACE IMPEDANCE OF A THIN PLASMA SHEET

Prepared by

T. M. Smith and K. E. Golden
Plasma Research Laboratory

AEROSPACE CORPORATION
El Segundo, California

Contract No. AF 04(695)-269

7 October 1963

Prepared for

COMMANDER SPACE SYSTEMS DIVISION
UNITED STATES AIR FORCE
Inglewood, California

SSD-TDR-63-261

Report No.
TDR-269(4280-10)-1

SURFACE IMPEDANCE OF A THIN PLASMA SHEET

Prepared by:

T.M. Smith

K.E. Golden

Approved by:

R.H. Huddlestone, Head
Plasma Physics Department

R.X. Meyer, Director
Plasma Research Laboratory

This technical documentary report has been reviewed and is approved for publication and dissemination. The conclusions and findings contained herein do not necessarily represent an official Air Force position.

For Space Systems Division
Air Force Systems Command:

G.S. Lewis, Jr., Major

AEROSPACE CORPORATION
El Segundo, California

ABSTRACT

An analysis is made of electromagnetic propagation through a homogeneous, isotropic, and slightly ionized plasma slab. Exact solutions for the reflection and transmission coefficients are given as functions of slab thickness, incident angle, and plasma wave number. Two approximations are introduced which allow the plasma slab to become a thin current sheet. When the approximations are valid, the reflection and transmission coefficients for the thin plasma are a function of the sheet surface impedance only. This surface impedance is related simply to the product of the sheet thickness and conductivity.

CONTENTS

FIGURES

ACKNOWLEDGEMENT

The authors would like to thank Drs. R. H. Huddlestone and E. C. Taylor for many helpful discussions during the course of this work. They also wish to acknowledge the assistance of E. S. Ozaki in processing the computer data and constructing the figures, and of Miss H.J. Sommers and Mrs. E. F. Grizzle in preparing the manuscript.

I. INTRODUCTION

Propagation of electromagnetic (EM) waves through plasma slabs is a topic of current interest. This situation is encountered in both plasma diagnostics and re-entry communications. A regime of particular interest in the re-entry application is that in which (1) the plasma wavenumber is large compared with the incident wavenumber, and (2) the slab thickness is small compared with the plasma skin depth. Such a thin plasma slab is shown to behave electrically as an inductive current sheet, having a lumped surface impedance consisting of an inductance in series with a resistance.

The EM properties of a thin plasma sheet can be represented completely by a surface impedance. That is to say, current sheets with the same surface impedance will produce the same EM reflection and transmission coefficients. This behavior of a thin plasma sheet enables it to be simulated easily.[1,2] A plane of equally spaced conducting wires and a thin conducting sheet with small apertures are two examples of current sheets with analogous surface impedances.[2-4] Also, arrays of fast switching microwave diodes behave as inductive current sheets over a large range of bias voltages. Switching diodes can be used to represent transient plasma sheets by varying the diode bias as a function of time.

Although this investigation has been motivated principally by plasma simulation interests,[5] this paper is concerned mainly with the EM mathematical model for a thin plasma sheet. The present analysis begins with the derivation of the reflection and transmission coefficients for an EM wave obliquely incident upon a plasma slab of finite thickness. Two approximations of these coefficients are examined.[6]

The first approximation assumes that the plasma wavenumber is large compared with the incident wavenumber. This restriction causes the refraction angle in the plasma to be near zero for all values of the incident angle and, in addition, simplifies the plasma wavenumber expression.

The second approximation involves the additional assumption that the slab thickness is small compared with the plasma skin depth. These requirements characterize a thin plasma sheet. A number of plots demonstrate the differences between the approximate and exact solutions.

Plasma surface impedance and conductivity are discussed in Section IV. A further examination of EM waves obliquely incident upon a thin plasma sheet is made from a different viewpoint. Starting with Maxwell's equations, the thin slab problem is resolved by applying the restrictions studied earlier as jump boundary conditions. In this approximation the reflection and transmission coefficients are seen clearly to be a function of only the sheet surface impedance.

All plasmas discussed in this paper are assumed to be homogeneous, isotropic and slightly ionized. Collision effects due to electron-neutral collisions are assumed to be velocity independent. No external magnetic fields are considered.

II. EXACT SOLUTION

In this section a plane EM wave obliquely incident upon a plasma slab is analyzed. When oblique incidence is encountered, it is advantageous to separate the radiation into perpendicular and parallel polarized components. Often the perpendicular polarization is called the transverse electric (TE) mode and has the electric field vector perpendicular to the plane of incidence. The plane of incidence is defined by the normal to the slab interface and the incident ray (the two sides which form angle θ in Fig. 1). Parallel polarization is also called the transverse magnetic (TM) mode and has the electric field vector parallel to the plane of incidence.

For the TE mode the appropriate plane wave solutions[7] to Maxwell's equations for the electric field vectors in the three regions of Fig. 1 are

$$\bar{E}_a = \bar{a}_x \left\{ E_1 \exp(-jk_o z \cos\theta) + E_2 \exp(jk_o z \cos\theta) \right\} \exp[j(\omega t - k_o y \sin\theta)] \tag{1}$$

$$\bar{E}_b = \bar{a}_x \left\{ E_3 \exp(-jk_p z \cos\phi) + E_4 \exp(jk_p z \cos\phi) \right\} \exp[j(\omega t - k_p y \sin\phi)] \tag{2}$$

$$\bar{E}_c = \bar{a}_x \left\{ E_5 (-jk_o \cos\theta) \right\} \exp[j(\omega t - k_o y \sin\theta)] \tag{3}$$

where

$$k_o = \omega(\mu_o \varepsilon_o)^{1/2} \qquad \text{(free space wavenumber)} \tag{4}$$

$$k_p = k_o \left(1 - \frac{j\sigma}{\omega\varepsilon}\right)^{1/2} \qquad \text{(plasma wavenumber)} \tag{5}$$

$$\sigma = \frac{\omega_p^2 \varepsilon_o}{\nu_c + j\omega} \qquad \text{(plasma conductivity)} \tag{6}$$

ω = incident frequency (rad/sec)

ω_p = plasma frequency (rad/sec)

ν_c = collision frequency (rad/sec)

ε_o = permittivity of free space

μ_o = permeability of free space

$\bar{a}_x$ = unit vector in x direction

θ = angle of incidence

ϕ = angle of refraction

t = time

x,y,z = coordinates

The letter subscripts refer to the total field in a given region, and the numeral subscripts designate in-going and out-going waves as shown in Fig. 1. All units are in the MKS system.

Two boundary conditions must be satisfied at each interface:

$$\left.\begin{aligned} \bar{E}_a &= \bar{E}_b \\ \frac{\partial \bar{E}_a}{\partial z} &= \frac{\partial \bar{E}_b}{\partial z} \end{aligned}\right\} \text{at } z = 0$$

$$\left.\begin{aligned} \bar{E}_b &= \bar{E}_c \\ \frac{\partial \bar{E}_b}{\partial z} &= \frac{\partial \bar{E}_c}{\partial z} \end{aligned}\right\} \text{at } z = d$$

These conditions require the tangential components of the electric and magnetic fields to be continuous across each interface. In addition, Snell's law is needed to satisfy phase continuity at the boundaries and is stated as

$$\cos \phi = \left[1 - \left(\frac{k_o}{k_p} \right)^2 \sin^2 \theta \right]^{1/2} \tag{7}$$

When the boundary conditions are applied to Eqs. (1)-(3), the following set of equations is obtained

$$\begin{pmatrix} E_1 \\ E_1 \\ 0 \\ 0 \end{pmatrix} = \begin{pmatrix} -1 & 1 & 1 & 0 \\ 1 & A & -A & 0 \\ 0 & 1/B & B & -C \\ 0 & -1/B & B & C/A \end{pmatrix} \begin{pmatrix} E_2 \\ E_3 \\ E_4 \\ E_5 \end{pmatrix} \tag{8}$$

where

$$A = \frac{k_p \cos\phi}{k_o \cos\theta} \tag{9}$$

$$B = \exp(jk_p d \cos\phi) \tag{10}$$

$$C = \exp(-jk_o d \cos\theta) \tag{11}$$

With the aid of Cramer's rule, the reflection and transmission coefficients are found from Eq. (8).

$$R(\perp) = \frac{E_2}{E_1}$$

$$R(\perp) = \frac{\frac{j}{2}\left(\frac{k_o \cos\theta}{k_p \cos\phi} - \frac{k_p \cos\phi}{k_o \cos\theta}\right) \sin\,[k_p d \cos\,\phi]}{\cos[k_p d \cos\phi] + \frac{j}{2}\left(\frac{k_o \cos\theta}{k_p \cos\phi} + \frac{k_p \cos\phi}{k_o \cos\theta}\right) \sin[k_p d \cos\phi]} \tag{12}$$

$$T(\perp) = \frac{E_5}{E_1}$$

$$T(\perp) = \frac{\exp(jk_o d \cos\theta)}{\cos[k_p d \cos\phi] + \frac{j}{2}\left(\frac{k_o \cos\theta}{k_p \cos\phi} + \frac{k_p \cos\phi}{k_o \cos\theta}\right) \sin[k_p d \cos\phi]} \tag{13}$$

These are the coefficients for the perpendicular polarization (TE mode).

A similar procedure involving the magnetic field vectors leads to the coefficients for the TM mode. The proper solutions[7] to Maxwell's equations for the magnetic field vectors in the three regions of Fig. 1 are

$$\bar{H}_a = \bar{a}_x \left\{ H_1 \exp(-jk_o z \cos\theta) + H_2 \exp(jk_o z \cos\theta) \right\} \exp[j(\omega t - k_o y \sin\theta)] \tag{14}$$

$$\bar{H}_b = \bar{a}_x \left\{ H_3 \exp(-jk_p z \cos\phi) + H_4 \exp(jk_p z \cos\phi) \right\} \exp[j(\omega t - k_p y \sin\phi)] \tag{15}$$

$$\bar{H}_c = \bar{a}_x \left\{ H_5 \exp(-jk_o z \cos\theta) \right\} \exp[j(\omega t - k_o y \sin\theta)] \tag{16}$$

The notation is the same as in the first case.

For the TM mode the boundary conditions which insure tangential continuity of the field across the interfaces are

$$\left.\begin{aligned} \bar{H}_a &= \bar{H}_b \\ \frac{1}{j\omega\varepsilon_o} \frac{\bar{H}_a}{\partial z} &= \frac{1}{\sigma + j\omega\varepsilon_o} \frac{\bar{H}_b}{\partial z} \end{aligned}\right\} \text{ at } z = 0 \tag{17}$$

$$\left.\begin{aligned} \bar{H}_b &= \bar{H}_c \\ \frac{1}{\sigma + j\omega\varepsilon_o} \frac{\partial\bar{H}_b}{\partial z} &= \frac{1}{j\omega\varepsilon_o} \frac{\partial\bar{H}_c}{\partial z} \end{aligned}\right\} \text{ at } z = d \tag{18}$$

Snell's law has the same form as Eq. (7).

Applying the boundary conditions of Eqs. (17) and (18) to the plane wave solutions of Eqs. (14)-(16) leads to

$$\begin{pmatrix} H_1 \\ H_1 \\ 0 \\ 0 \end{pmatrix} = \begin{pmatrix} -1 & 1 & 1 & 0 \\ 1 & D & -D & 0 \\ 0 & 1/B & B & -C \\ 0 & -1/B & B & C/D \end{pmatrix} \begin{pmatrix} H_2 \\ H_3 \\ H_4 \\ H_5 \end{pmatrix} \tag{19}$$

where

$$D = \frac{k_o \cos\phi}{k_p \cos\theta}$$

and B and C are given by Eqs. (10) and (11).

The reflection and transmission coefficients are obtained in the same manner as in the previous case

$$R(\parallel) = \frac{E_2}{E_1} = \frac{-H_2}{H_1} \tag{20}$$

$$R(\parallel) = \frac{\frac{j}{2}\left(\frac{k_o \cos\phi}{k_p \cos\theta} - \frac{k_p \cos\theta}{k_o \cos\phi}\right)\sin\left[k_p d \cos\phi\right]}{\cos\left[k_p d \cos\phi\right] + \frac{j}{2}\left(\frac{k_o \cos\phi}{k_p \cos\theta} + \frac{k_p \cos\theta}{k_o \cos\phi}\right)\sin\left[k_p d \cos\phi\right]}$$

$$T(\parallel) = \frac{E_5}{E_1} = \frac{H_5}{H_1} \tag{21}$$

$$T(\parallel) = \frac{\exp(jk_o d \cos\theta)}{\cos\left[k_p d \cos\phi\right] + \frac{j}{2}\left(\frac{k_o \cos\phi}{k_p \cos\theta} + \frac{k_p \cos\theta}{k_o \cos\phi}\right)\sin\left[k_p d \cos\phi\right]}$$

These are the coefficients for the TM mode, and they differ from those for the TE mode only in the location of the quotient ($\cos\theta/\cos\phi$).

Equations (12), (13), (20), and (21) were programmed in the Fortran notation and evaluated on the 7090 computer. Figures 2-7 demonstrate the effect of the incident angle on the reflection and transmission coefficients. The coefficients are plotted as a function of slab thickness, $k_o d$, for various values of θ, and fixed values of plasma ratios, ω_p/ω, and collision ratios, ν_c/ω.

For the lossless case ($\nu_c/\omega = 0$), the zeros of the reflection coefficient are given by the expression

$$k_o d = \frac{n\pi}{\left[\cos^2\theta - \left(\omega_p/\omega\right)^2\right]^{1/2}}, n = 1,2,3 \cdots$$

When the denominator of this expression is zero, a critical angle occurs. The oscillations in the coefficients cease when angle θ exceeds the critical value.

III. APPROXIMATE SOLUTIONS

Two sets of approximate solutions for Eqs. (12), (13), (20), and (21) are examined in this section. For the first approximation, it is assumed that the plasma wavenumber is much larger than the incident wavenumber.

$$|k_p|^2 \gg k_o^2 \tag{22}$$

This restriction allows Eq. (5) to become

$$k_p' = k_o \left[\frac{-j\omega_p^2}{\omega\left(\nu_c + j\omega\right)} \right]^{1/2} \tag{23}$$

where k_p' is the asymptotic form of the plasma wavenumber. As $|k_p|^2$ becomes large, the refraction angle, ϕ, approaches a constant value of zero.

$$\cos \phi \approx 1 \tag{24}$$

$$\phi \approx 0$$

This condition follows from Eqs. (7) and (22).

The significance of this approximation lies in the simplified form of the wave solution in the plasma region as given in Eqs. (2) and (15). The elimination of the ϕ dependence represents an appreciable simplification when more complicated geometries are encountered.

If inequality (22) holds, the reflection and transmission coefficients become

$$R'(\perp) = \frac{\left(\dfrac{k_o \cos\theta}{k_p'} - \dfrac{k_p'}{k_o \cos\theta}\right) \sin[k_p' d]}{\cos[k_p' d] + \dfrac{j}{2}\left(\dfrac{k_o \cos\theta}{k_p'} + \dfrac{k_p'}{k_o \cos\theta}\right) \sin[k_p' d]} \tag{25}$$

$$T'(\perp) = \frac{\exp(jk_o d \cos\theta)}{\cos[k_p' d] + \dfrac{j}{2}\left(\dfrac{k_o \cos\theta}{k_p'} + \dfrac{k_p'}{k_o \cos\theta}\right) \sin[k_p' d]} \tag{26}$$

$$R'(||) = \frac{\left(\dfrac{k_o}{k_p' \cos\theta} - \dfrac{k_p' \cos\theta}{k_o}\right) \sin[k_p' d]}{\cos(k_p' d] + \dfrac{j}{2}\left(\dfrac{k_o}{k_p' \cos\theta} + \dfrac{k_p' \cos\theta}{k_o}\right) \sin[k_p' d]} \tag{27}$$

$$T'(||) = \frac{\exp(jk_o d \cos\theta)}{\cos[k_p' d] + \dfrac{j}{2}\left(\dfrac{k_o}{k_p' \cos\theta} + \dfrac{k_p' \cos\theta}{k_o}\right) \sin[k_p' d]} \tag{28}$$

where primed quantities refer to the first approximation. The difference between approximate and exact reflection and transmission coefficients is shown in Figs. 8 and 9. These errors are measured by the relationships

$$
\begin{aligned}
\Delta_R(\perp) &= R'(\perp) - R(\perp) \\
\Delta_T(\perp) &= T'(\perp) - T(\perp) \\
\Delta_R(||) &= R'(||) - R(||) \\
\Delta_T(||) &= T'(||) - T(||)
\end{aligned}
\tag{29}
$$

and are plotted as a function of align $k_o d$ for various values of θ with plasma and collision ratios fixed. In Fig. (8) it is noted that the cos θ term reduces the effect of $|k_p|^2$ being large for the TM mode and enhances this effect for the TE mode. As θ approaches 90°, the TM mode error increases and the TE mode error decreases.

Two assumptions are involved in the second approximation:[8,9] (1) the plasma wavenumber is large compared with incident wave number,

$$|k_p|^2 \gg k_o^2 \tag{22}$$

(2) the slab thickness is small compared to the plasma skin depth such that the product

$$k_p d \ll 1 \tag{30}$$

The first assumption was discussed in the preceding paragraphs. The second assumption allows the trigonometric functions to be replaced by the first term in their series expansions.

The second approximate solution represents the coefficients for a thin current sheet which is the principle topic under consideration here. For any plasma operating in cutoff ($k_p > k_o$), the situation of primary interest is the one which can be approximated by a thin current sheet. Most of the other cases are not of interest, because the transmission coefficient is negligible.

If $k_p d$ become much less than unity in Eqs. (25)-(28), the coefficients for the thin plasma sheet are found to be

$$R''(\perp) = \frac{-1}{1 + \dfrac{2k_o \cos\theta}{jk_p'^2 d}} \tag{31}$$

$$T''(\perp) = \frac{1}{1 + j\dfrac{k_p'^2 d}{2k_o \cos\theta}} \tag{32}$$

$$R''(\parallel) = \frac{-1}{1 + \dfrac{2k_o}{jk_p'^2 d \cos\theta}} \tag{33}$$

$$T''(\parallel) = \frac{1}{1 + j\dfrac{k_p'^2 \cos\theta}{2k_o}} \tag{34}$$

Equations (33) and (34), the TM mode coefficients, are not valid as θ approaches 90 deg. This follows from the discussion concerning the angular error for the first approximation. The correct limit for the TM mode coefficients can be obtained by analyzing Eqs. (20) and (21). From this analysis, it is found that the transmission coefficient approaches zero instead of one and that the reflection coefficient is greater than zero.

Figures (10a) and (10b) are plots of the magnitude and phase for the thin sheet coefficients. It should be noted that additional nomenclature has been introduced. From Eq. (23)

$$\frac{j\,k_p'^2\,d}{k_o} = \frac{W^2 D}{(V + j)} \tag{35}$$

where

$$W = \frac{\omega_p}{\omega} \quad \text{(plasma ratio)} \tag{36}$$

$$V = \frac{\nu_c}{\omega} \quad \text{(collision ratio)} \tag{37}$$

$$D = k_o d \quad \text{(length ratio)} \tag{38}$$

These dimensionless ratios are used for convenience. Angle θ does not appear directly in Figs. (10a) and (10b), but it can be introduced by modifying the length ratio to the forms

$$D_\perp = \frac{k_o d}{\cos\theta} \tag{39}$$

$$D_{||} = k_o d \cos\theta$$

The four coefficients of Eqs. (31) - (34) are reduced to two since the TE and TM modes are specified by replacing D with $D_\perp$ or $D_{||}$. Also, for ease in computation, the polar form of these equations is introduced so that

$$R'' = \frac{W^2 D}{2} \sin \psi \ \exp[j(\pi - 4) \tag{40}$$

$$T'' = \frac{\sin \psi}{\sin \delta} \ \exp[j(\delta - 4) \tag{41}$$

where

$$\tan \psi = \frac{1}{V + \frac{W^2 D}{2}} \tag{42}$$

$$\tan \delta = \frac{1}{V} \tag{43}$$

Errors in magnitude for the second approximation are seen by comparing Figs. (11) and (12) with (6) and (7). These figures demonstrate how error increases with increasing $k_o d$ and decreasing ω_p/ω . The effect of incident angle θ is shown for both polarizations.

IV. SURFACE IMPEDANCE AND CONDUCTIVITY

Surface impedance is defined[7] as

$$Z_s = \frac{\bar{E}_t}{\bar{J}_s} \tag{44}$$

where $\bar{E}_t$ is the tangential electric field parallel to an incident surface of a slab and $\bar{J}_s$ is the linear current density (A/m) flowing in the slab due to E_t. In terms of the current density, $\bar{J}$ (A/m^2), the surface current is

$$\bar{J}_s = \int_0^d (\bar{n} \times \bar{J}) \times d\bar{s} \tag{45}$$

where $\bar{n}$ is the unit normal to the incident surface, d is the slab thickness, and $d\bar{s}$ is the differential length in the direction of propagation. Ohm's law in terms of field quantities and conductivity is

$$\bar{E}_t = \frac{1}{\sigma} \bar{J} \tag{46}$$

If one substitutes Eq. (46) into (44)

$$Z_s = \frac{\bar{J}}{\sigma \bar{J}_s} \tag{47}$$

When the slab thickness is small compared to skin depth, the E field is constant through the slab in the direction of propagation. According to Ohm's law, the term $\bar{J}$ also is constant in the same region. When it is integrated over the thickness d,

$$\bar{J}_s = \bar{J} d \tag{48}$$

provided that ϕ is approximately zero for all θ. From Eqs. (47) and (48) the surface impedance of a thin sheet is

$$Z_s = \frac{1}{\sigma d} \quad \text{(ohms/sq)} \tag{49}$$

If the plasma is assumed to be slightly ionized and cold, its conductivity may be represented by the Lorentz gas model.[10] The governing equations for this model are

$$m \frac{d\bar{v}}{dt} + \nu_c \bar{v} = q\bar{E} \tag{50}$$

$$\bar{J} = \sigma \bar{E}$$

$$J = nq\bar{v}$$

where $\bar{v}$ = electron velocity, m = electron mass, q = electron charge, and n = electron density.

If the E field is assumed to have a time dependence $\exp(j\omega t)$, then the above equations lead to the expression

$$\sigma = \frac{nq^2}{m(\nu_c + j\omega)} \tag{51}$$

for the plasma conductivity. Usually the plasma frequency ω_p is introduced into Eq. (51) and

$$\sigma = \frac{\omega_p^2 \varepsilon_o}{\nu_c + j\omega} \tag{6}$$

where

$$\omega_p^2 = \frac{n\, q^2}{m\, \varepsilon_o} \tag{52}$$

This is the expression stated at the beginning in Eq. (6).

If one replaces the conductivity in Eq. (49), the surface impedance becomes

$$Z_s = \frac{\nu_c + j\omega}{\omega_p^2 \varepsilon_o\, d} = R_s + i\, X_s \tag{53}$$

which is a complex impedance having a resistive component

$$R_s = \frac{\nu_c}{\omega_p^2 \varepsilon_o\, d} \tag{54}$$

and a reactive component

$$X_s = \frac{1}{\omega_p^2 \varepsilon_o\, d} \tag{55}$$

Equation (53) conveniently is expressed as

$$Z_s = Z_o \frac{V + j}{W^2 D} \tag{56}$$

by introducing the dimensionless parameters of Eqs. (36) - (38), and Z_o is the intrinsic impedance of free space $(\mu_o/\varepsilon_o)^{1/2}$. By simple substitution it follows that

$$R_s = \frac{Z_o V}{W^2 D}$$

$$X_s = \frac{Z_o}{W^2 D} \tag{57}$$

The surface impedance of a thin sheet is given by Eq. (56) provided that assumptions (1) and (2) of the second approximation are valid. When one examines the components of the impedance, it is seen that the thin plasma behaves as an inductive current sheet.

V. JUMP PROBLEM

Now the thin sheet problem will be resolved by applying the restrictions of the second approximation directly to the plane wave solutions in regions a and c of Fig. 1. Imagine that the slab thickness d in Fig. 1 becomes small enough so that

$$k_p d \ll 1 \tag{30}$$

If inequality (30) is satisfied, the tangential E fields in regions a and c can be related as

$$\bar{n} \times (\bar{E}_a - \bar{E}_c) = 0 \tag{58}$$

When the E field impinges upon the thin slab, it causes a surface current to flow. This surface current is equal to the discontinuity in the tangential H field.

$$\bar{J}_s = \bar{n} \times (\bar{H}_a - \bar{H}_c) = \frac{1}{Z_s} \quad \bar{E}_t \tag{59}$$

The surface current may be replaced by the surface impedance and the E_t field in inequalities (22) and (30) are valid. Inequality (22) insures that ϕ is near zero.

It will be necessary to find H given E and E given H for the two polarizations. Maxwell's two curl equations furnish the required relations:

$$\begin{aligned} \bar{H} &= \frac{j}{\omega\mu_o} \quad \bar{\nabla} \times \bar{E} \\ \bar{E} &= \frac{1}{\sigma + j\omega\,\varepsilon_o} \bar{\nabla} \times \bar{H} \end{aligned} \tag{60}$$

First, the TE mode is considered. At $z = 0$ the jump conditions of Eqs. (58) and (59) are applied to the wave solutions of Eqs. (1) and (3), yielding

$$E_1 + E_2 = E_5 \tag{61}$$

$$\frac{\cos\theta}{Z_o}\left[E_1 - E_2 - E_5\right] = \frac{1}{Z_5} E_5 \tag{62}$$

where Z_o is the intrinsic impedance of free space. After algebraic manipulations of Eqs. (61) and (62), the reflection and transmission coefficients are found to be

$$R''(\perp) = \frac{-1}{1 + \dfrac{2 Z_s \cos\theta}{Z_o}} \tag{63}$$

$$T''(\perp) = \frac{1}{1 + \dfrac{Z_o}{2 Z_s \cos\theta}} \tag{64}$$

If Eqs. (31), (32), and (35) are compared with Eqs. (56), (63), and (64), the coefficients for the jump conditions are found to be the same as those for the second approximation.

In the case of TM mode the same procedure is followed. At $z = 0$ the jump conditions are applied to Eqs. (14) and (16) to obtain

$$- H_1 + H_2 = H_5 \tag{65}$$

$$H_1 + H_2 - H_5 = \frac{Z_o \cos\theta}{2 Z_s} H_5 \tag{66}$$

These two equations can be solved for the TM mode coefficients which are

$$R''(\perp) = \frac{-1}{1 + \dfrac{2\,Z_s}{Z_s \cos\theta}} \tag{67}$$

$$T''(\perp) = \frac{1}{1 + \dfrac{Z_o \cos\theta}{2\,Z_s}} \tag{68}$$

When one compares Eqs. (33), (34), and (35) with Eqs. (56), (67), and (68), it is found that the jump solution and the second approximate solution are the same for the TM mode also.

Thus, it has been shown that the reflection and transmission coefficients of the plasma sheet are a function of the sheet surface impedance only. This fact enables a straightforward simulation of the thin plasma by the methods mentioned in the introduction.

VI. CONCLUSION

The first topic was an analysis of the exact solutions for the reflection and transmission coefficients describing propagation through plasma slab of finite thickness. Figures 2-7 are plots of the exact solution for these coefficients indicating their dependence on the plasma ratio, collision ratio, length ratio, and incident angle. An expression for determining the zeros of the reflection coefficients for the lossless case is given. From the denominator of this expression it is possible to find the critical angle of a lossless plasma.

Two approximations of the exact solution are examined. The first approximation was based on the assumption that the plasma wave number is large compared to the incident wavenumber. This assumption made the problem independent of the refraction angle. Plots were given which showed the difference between the first approximation and the exact solution. As the angle of incidence approaches 90 deg the TM mode error increased and the TE mode error decreased. Error in both modes decreased for larger plasma ratios.

The second approximation, which characterizes the jump conditions, involves the added assumption that the sheet thickness is small compared to the plasma skin depth. Plots for the magnitude and phase of the jump coefficients are given, but these curves do not indicate directly the θ dependence. Additional plots, which show the θ-dependence for the second approximation, may be compared directly with the plots for the exact solution. Once again an increasing error is found for the TM mode as θ approaches 90 deg. Error was found to become larger as $k_o d$ increased and ω_p/ω decreased.

In the last section the problem was resolved using jump conditions. The results of the second approximation and the jump solution were compared and found to be identical. Therefore, it has been verified that a thin plasma sheet satisfying the jump conditions can be completely represented electrically by its surface impedance.

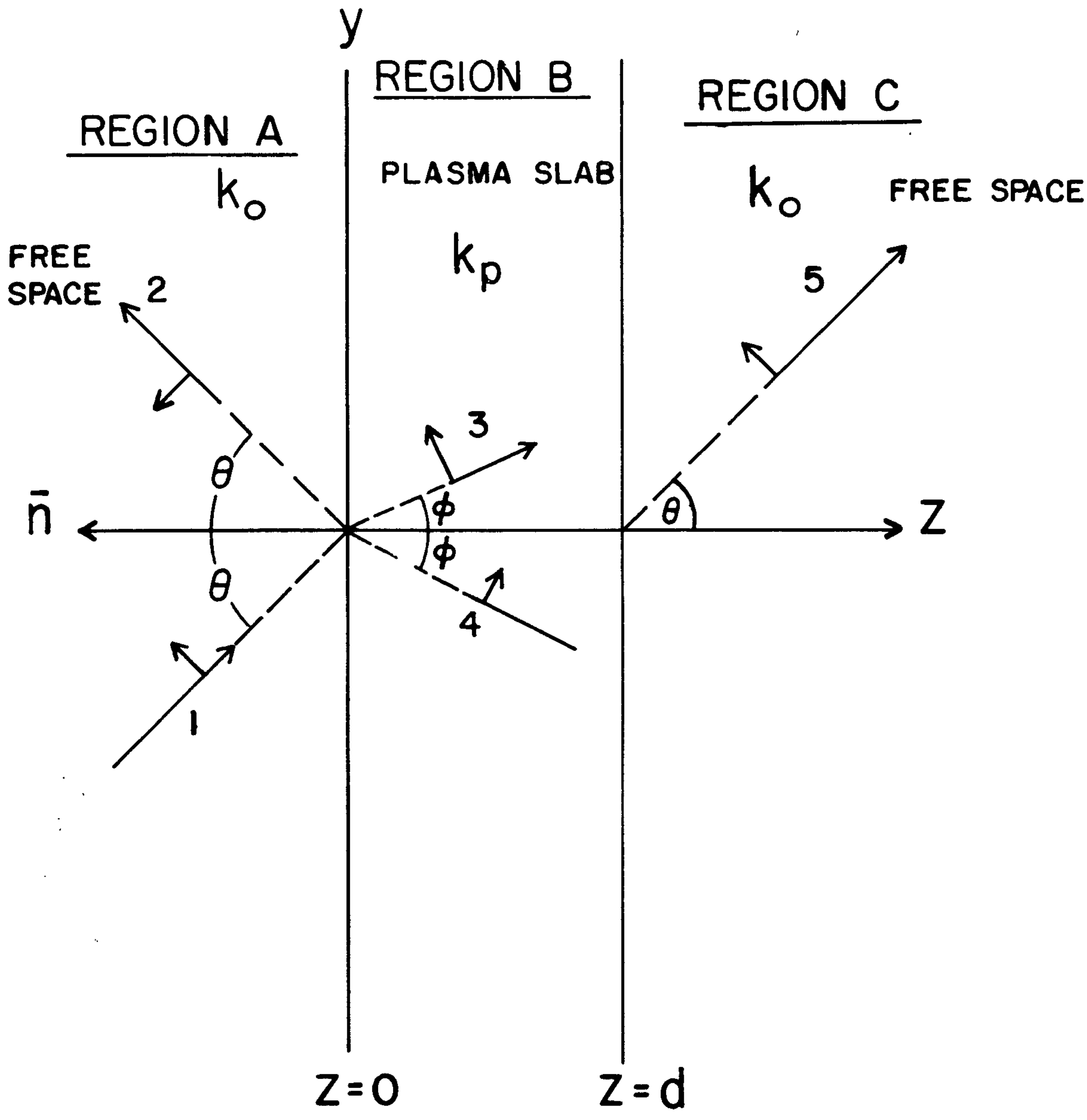

Fig. 1. Finite Plasma Slab

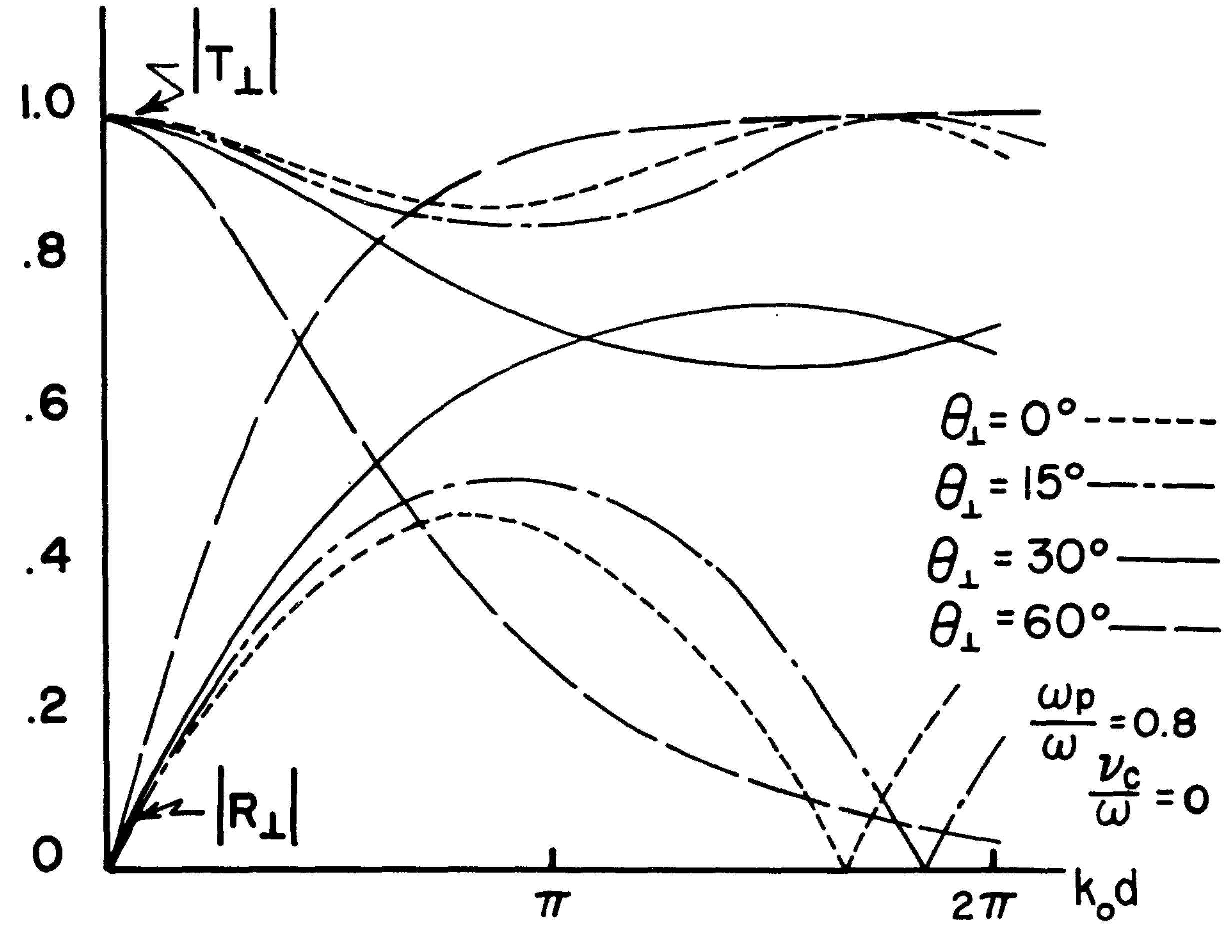

Fig. 2a. Exact Solution, above Cutoff, Lossless (TE Mode)

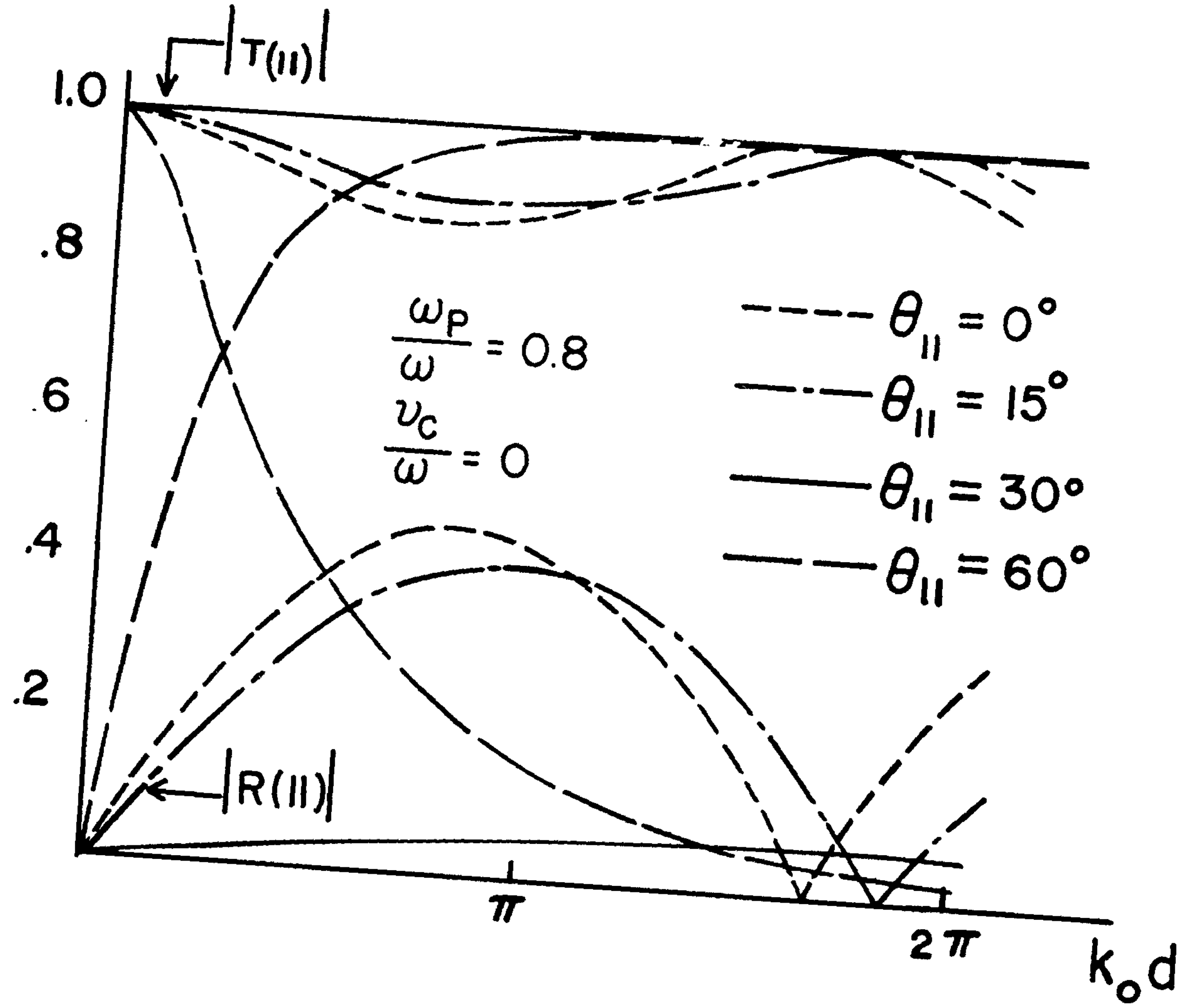

Fig. 2b. Exact Solution, above Cutoff, Lossless (TM Mode)

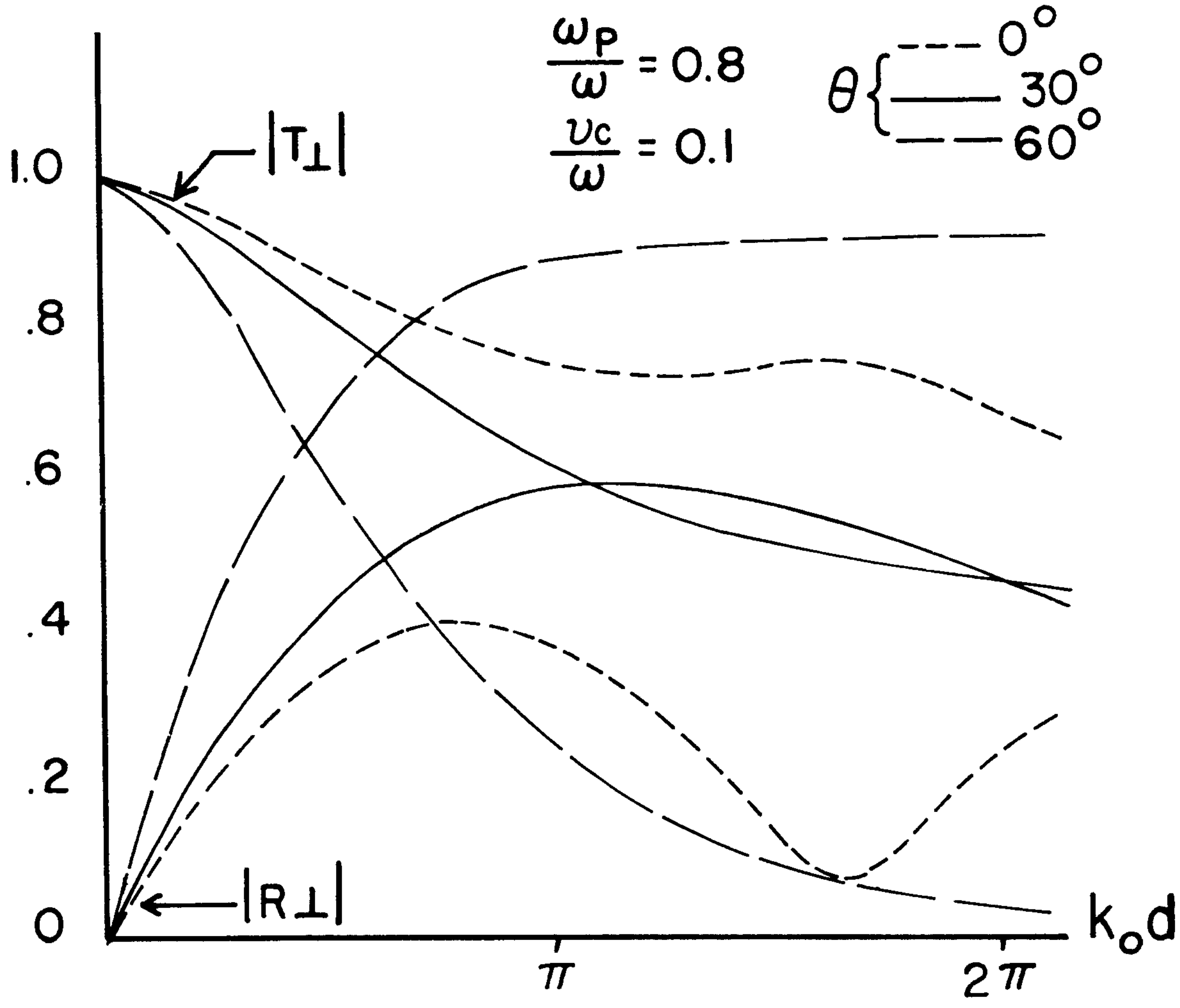

Fig. 5a. Exact Solution, above Cutoff, Lossy (TE Mode)

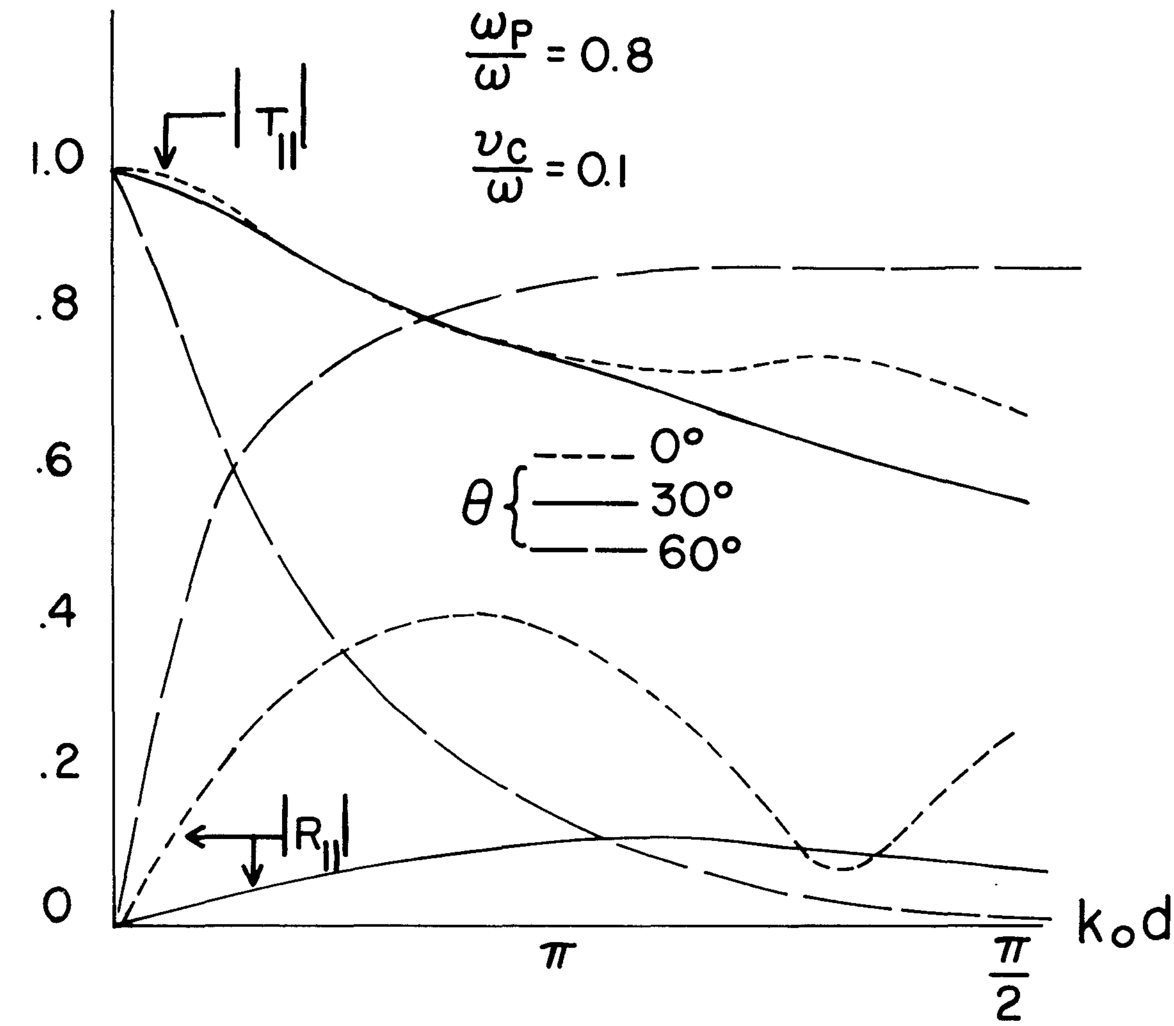

Fig. 3b, Exact Solution, above Cutoff, Lossy (TM Mode)

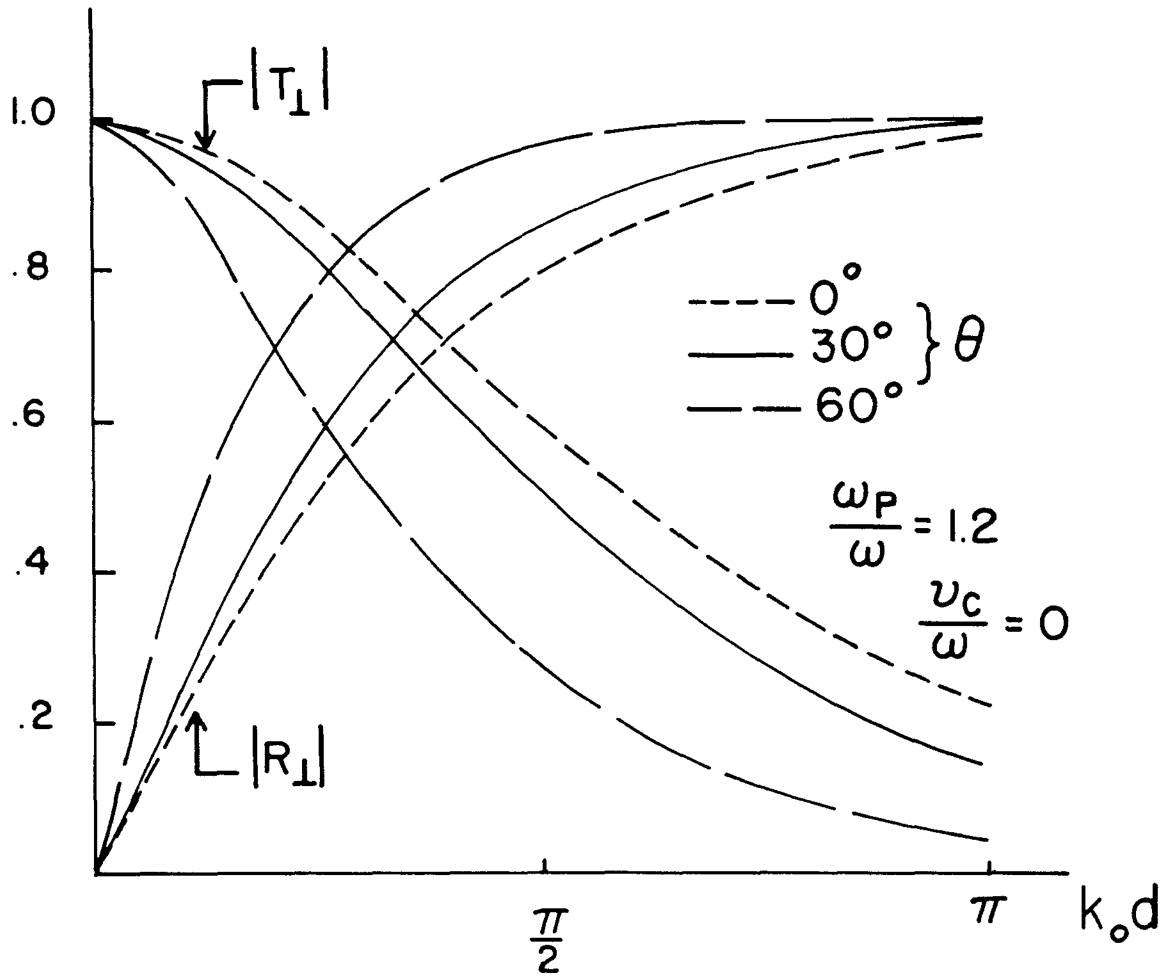

Fig. 4a. Exact Solution, below Cutoff, Lossless (TE Mode)

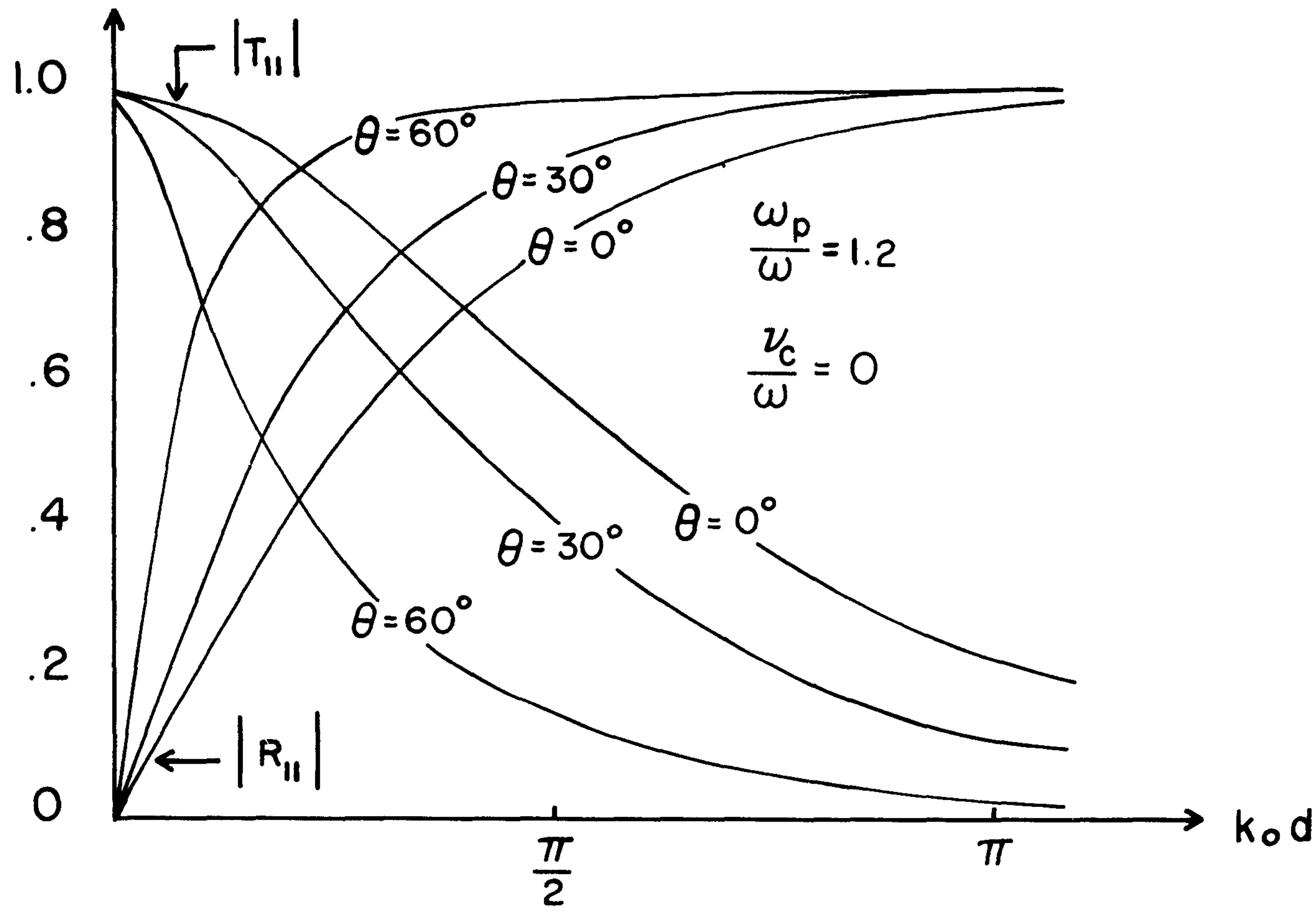

Fig. 4b. Exact Solution, below Cutoff, Lossless (TM Mode)

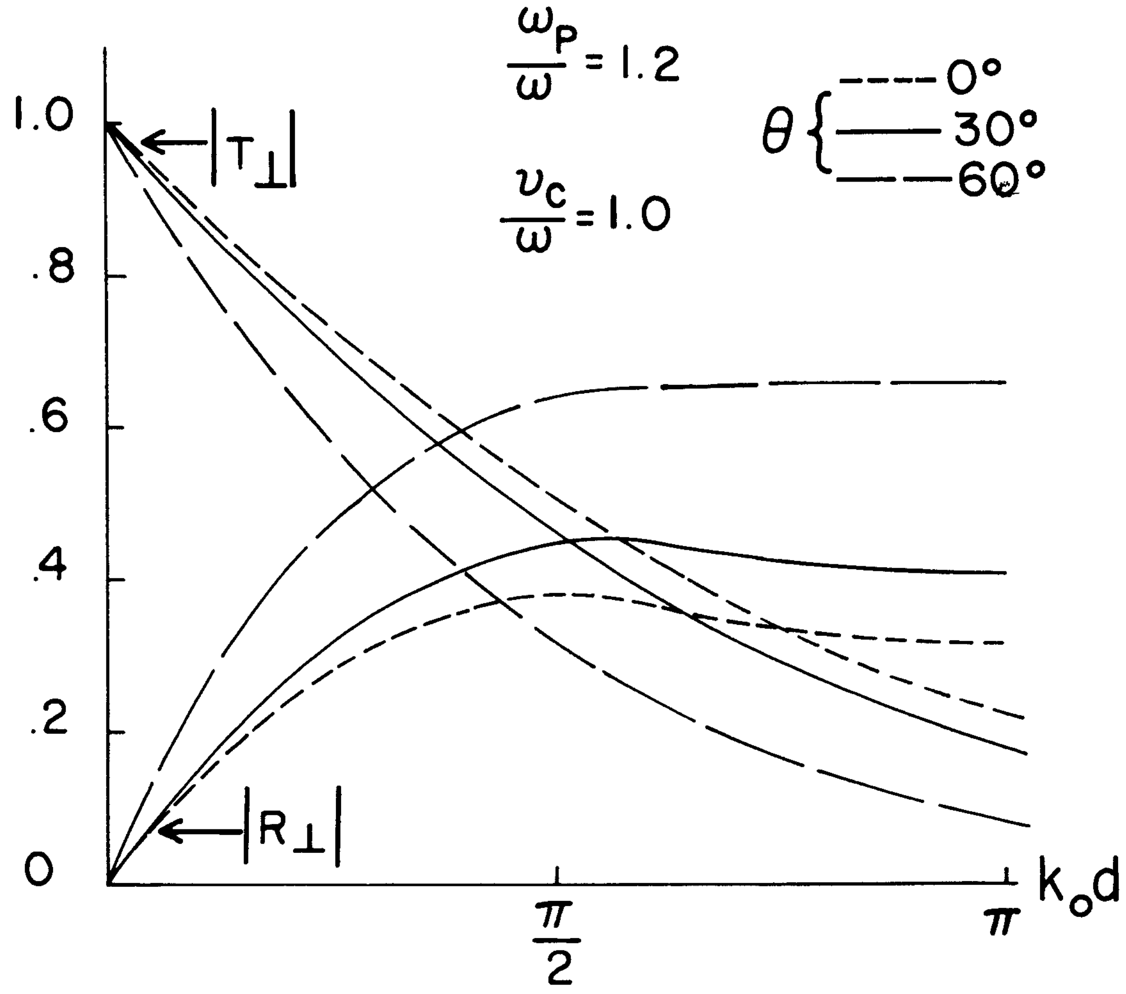

Fig. 5a. Exact Solution, below Cutoff, Lossy (TE Mode)

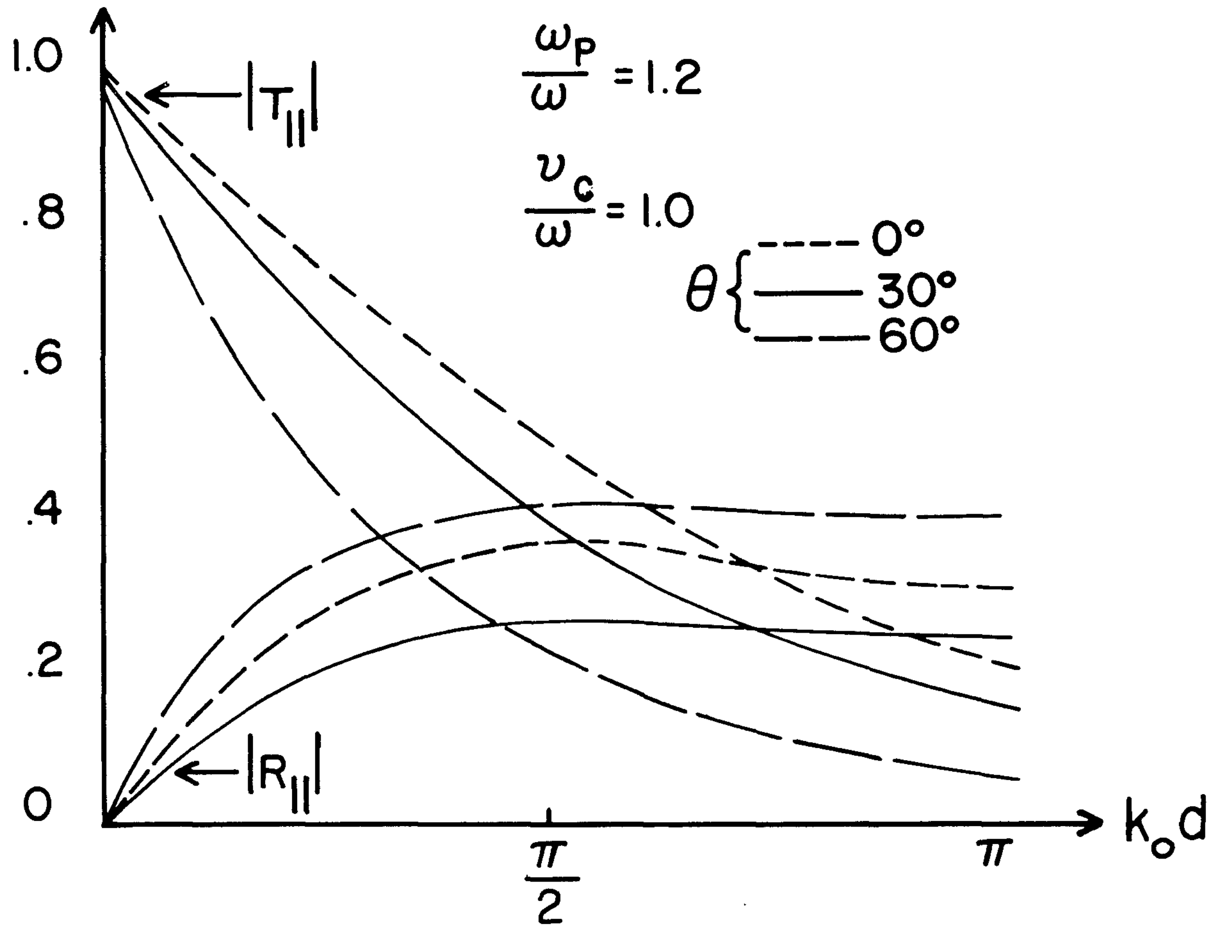

Fig. 5b. Exact Solution, below Cutoff, Lossy (TM Mode)

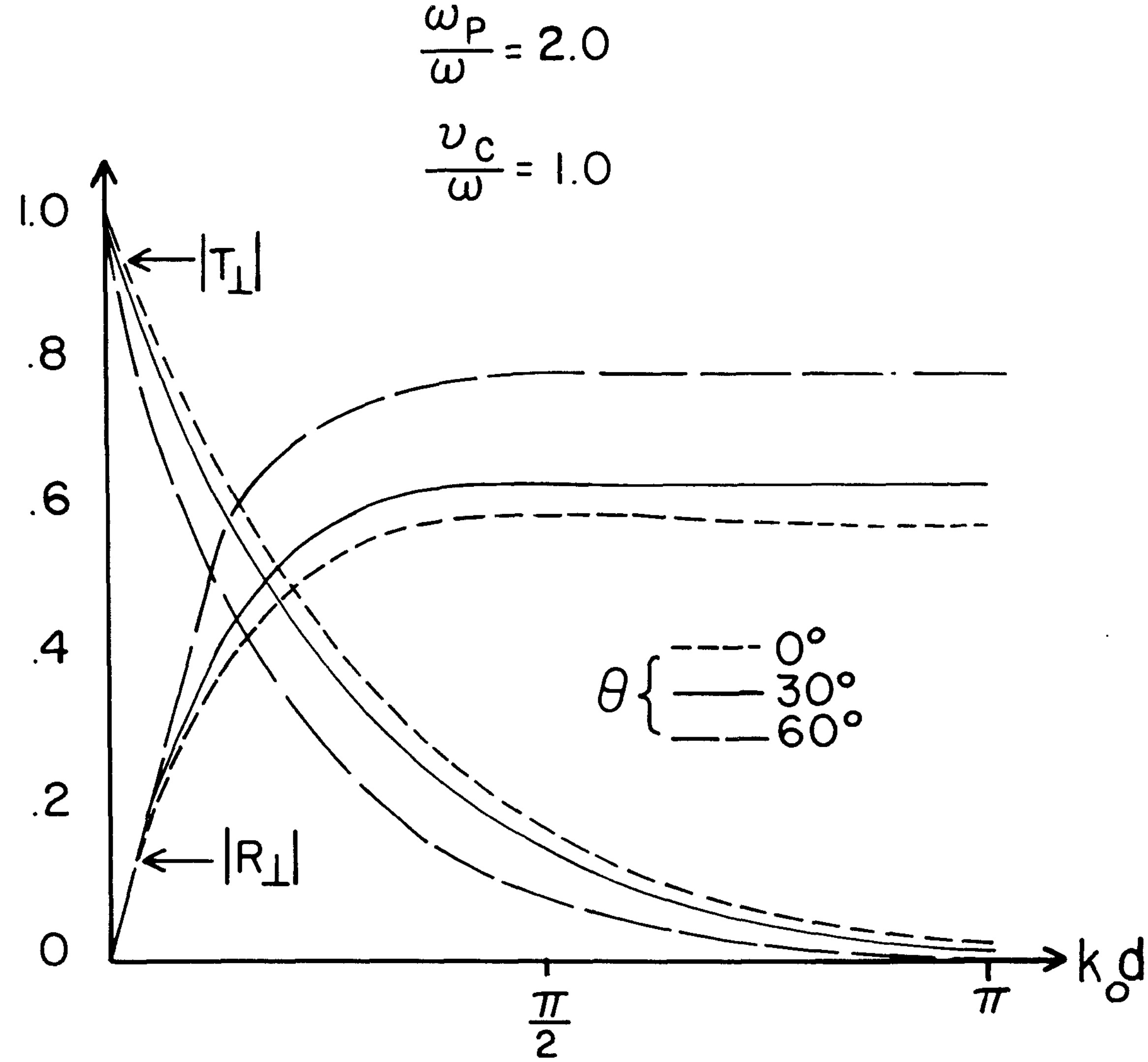

Fig. 6a. Exact Solution, below Cutoff, Lossy, $\omega_p/\omega = 2$ (TE Mode)

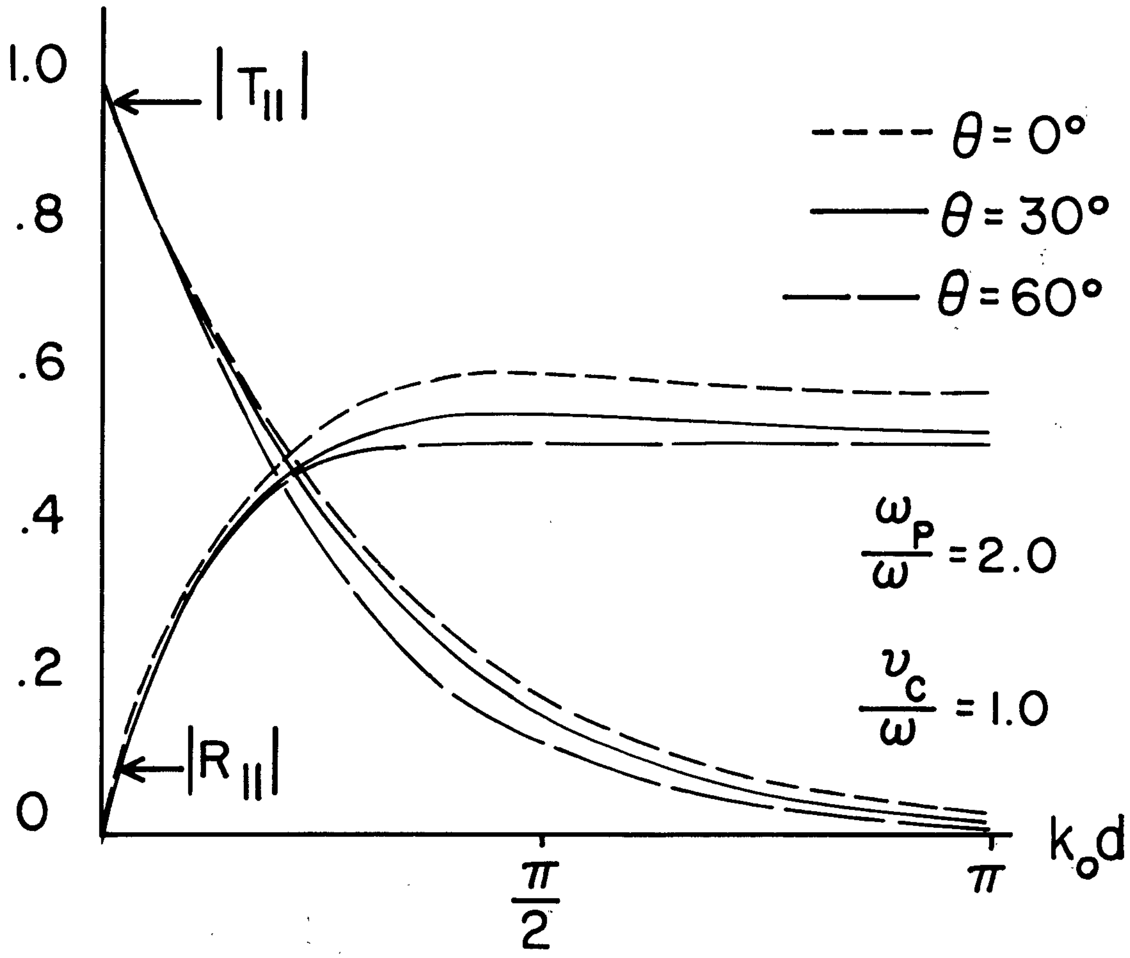

Fig. 6b. Exact Solution, below Cutoff, Lossy, $\omega_p/\omega = 2$ (TM Mode)

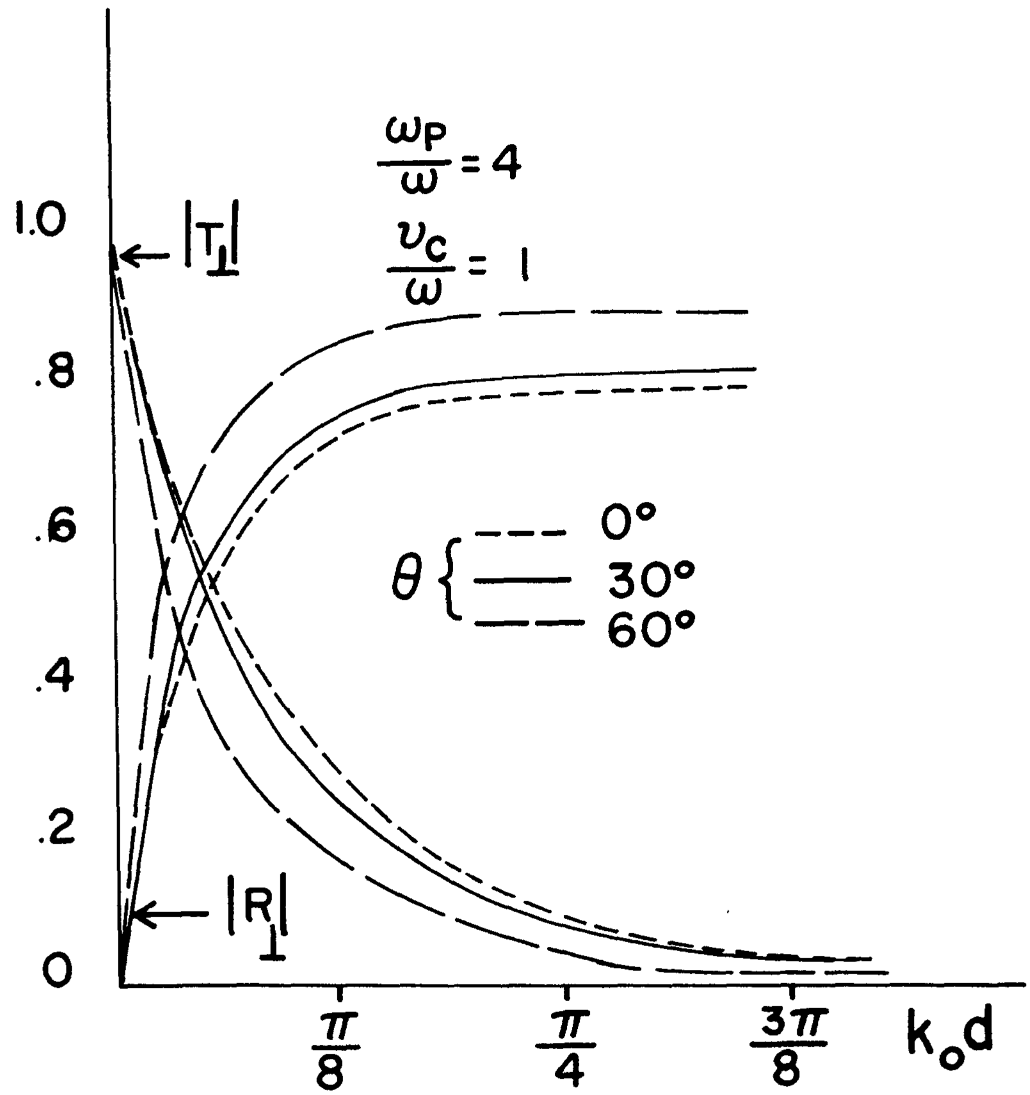

Fig. 7a. Exact Solution, below Cutoff, Lossy, $\omega_p/\omega = 4$ (TM Mode)

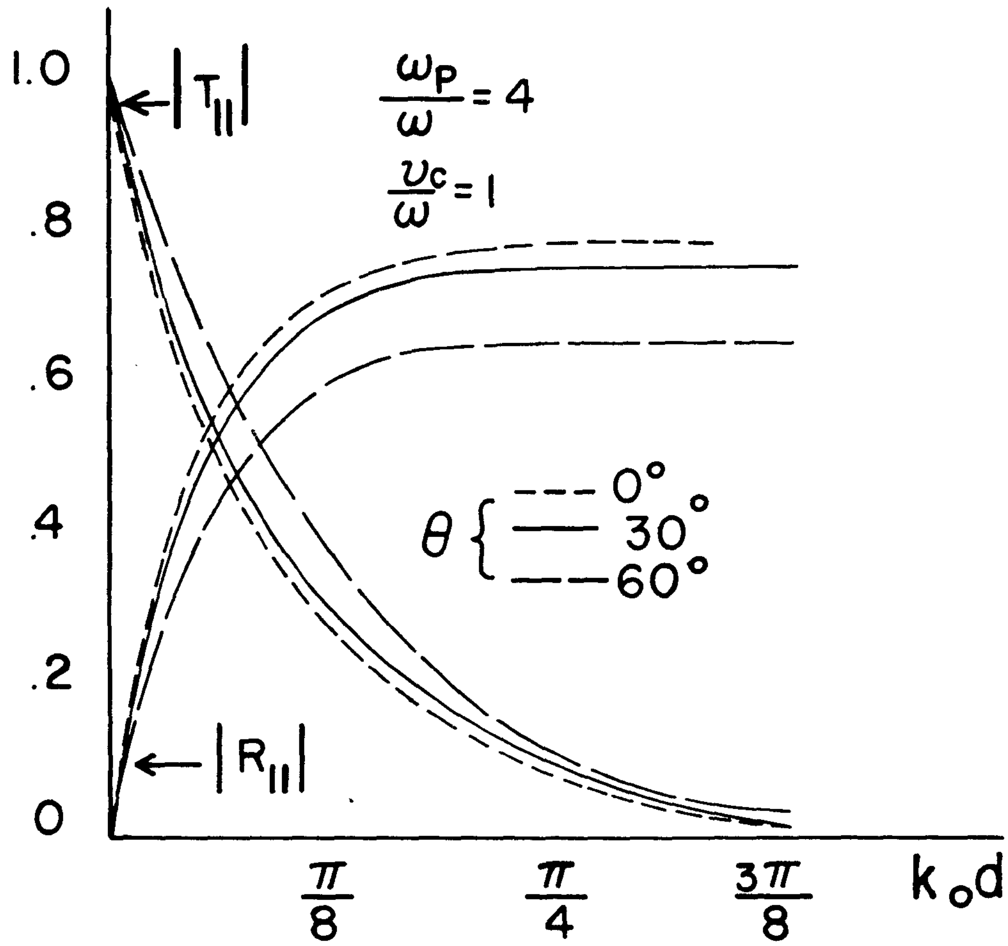

Fig. 7b. Exact Solution, below Cutoff, Lossy, $\omega_p/\omega = 4$ (TM Mode)

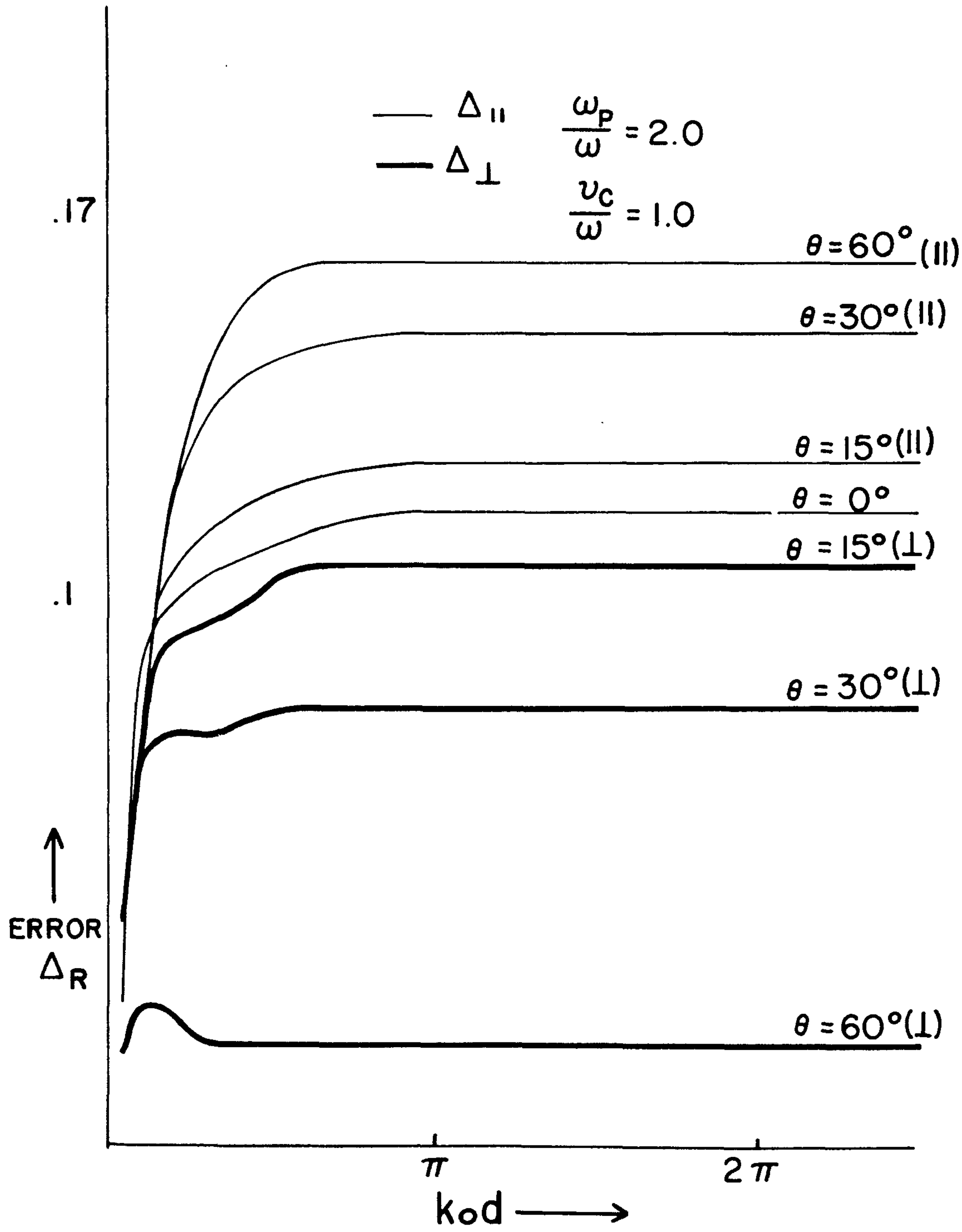

Fig. 8a. First Approximation Reflection Error ($\omega_p/\omega = 2$)

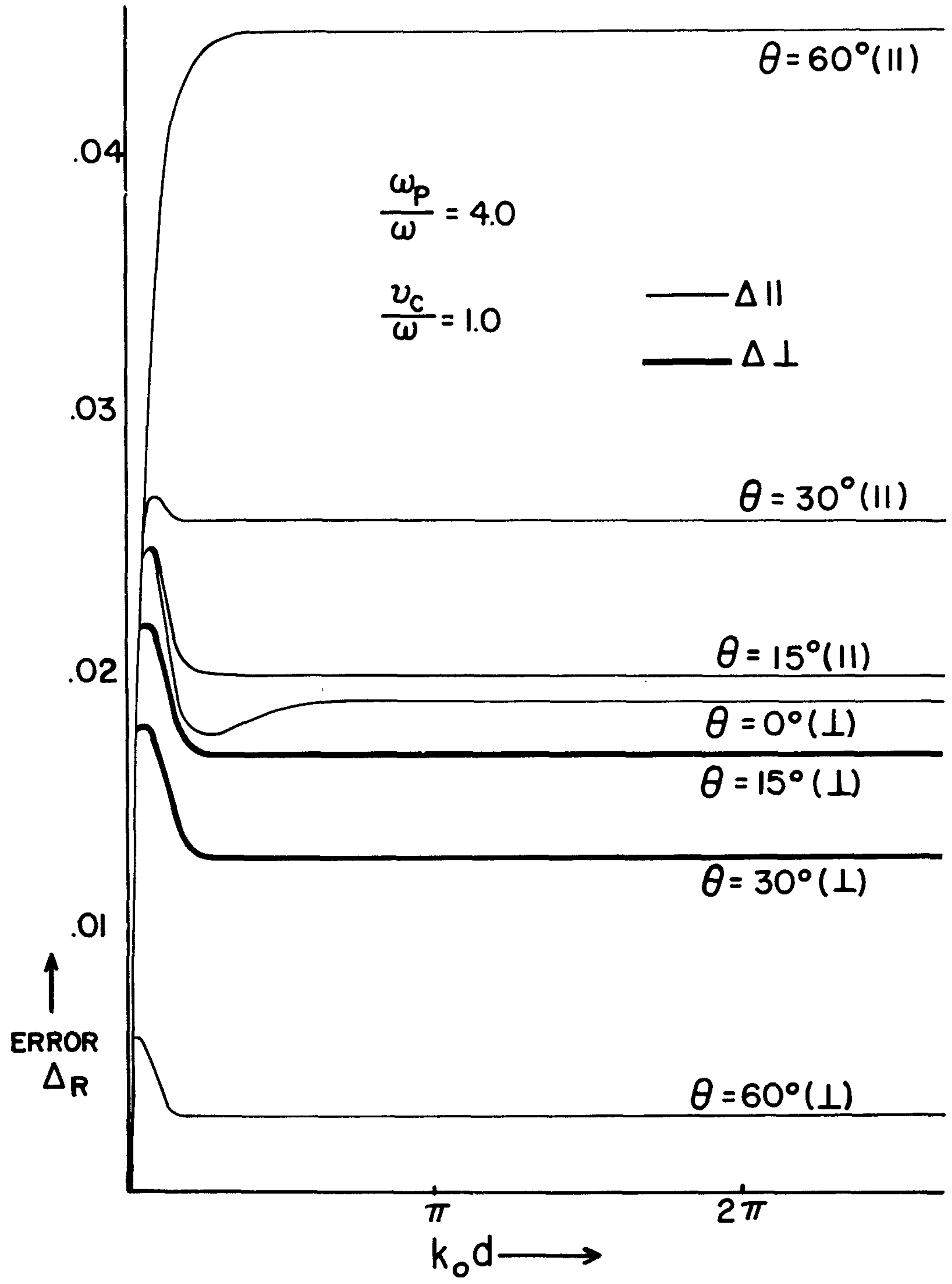

Fig. 8b. First Approximation Reflection Error (ω_p/ω - 4)

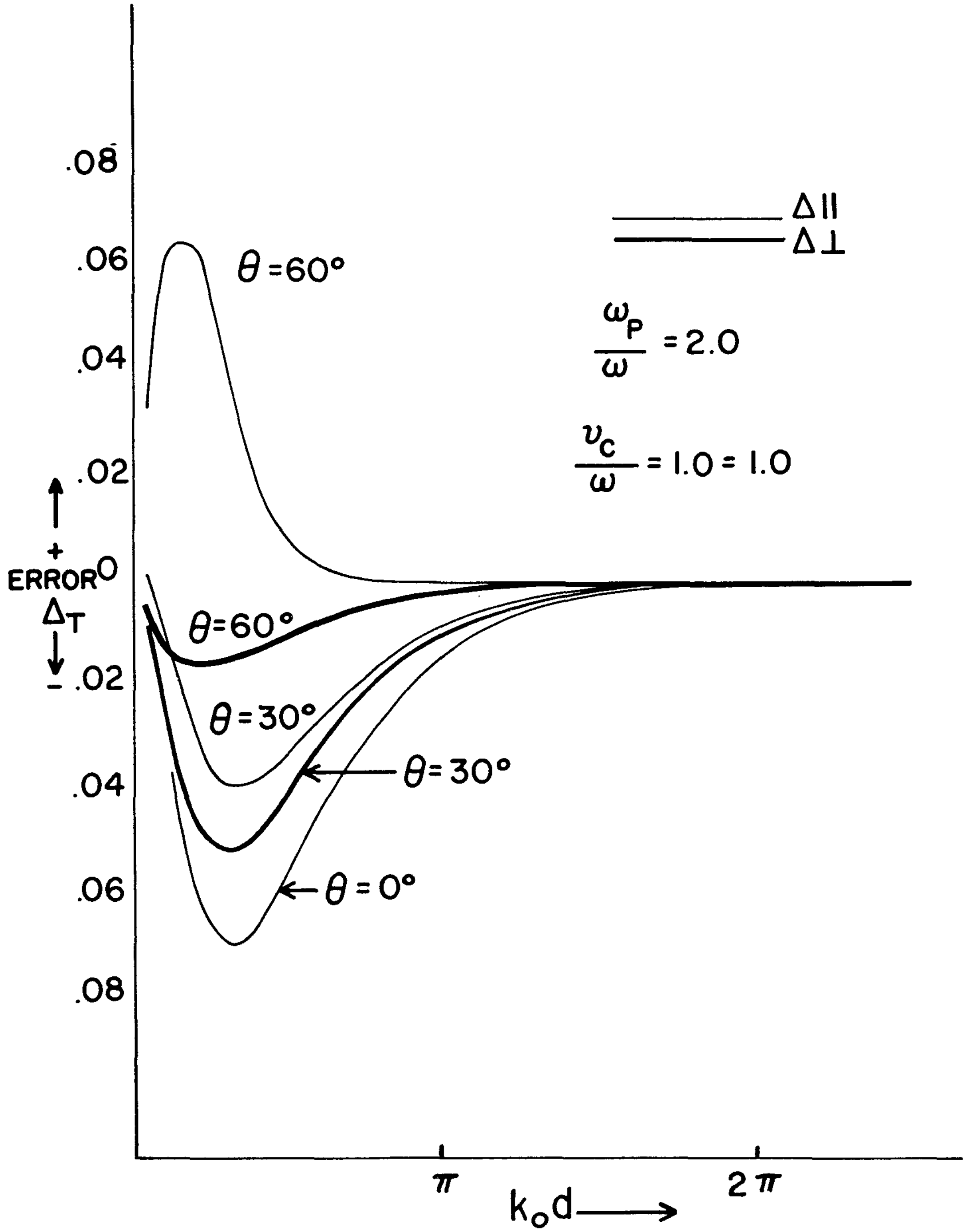

Fig. 9a. First Approximation Transmission Error ($\omega_p/\omega = 2$)

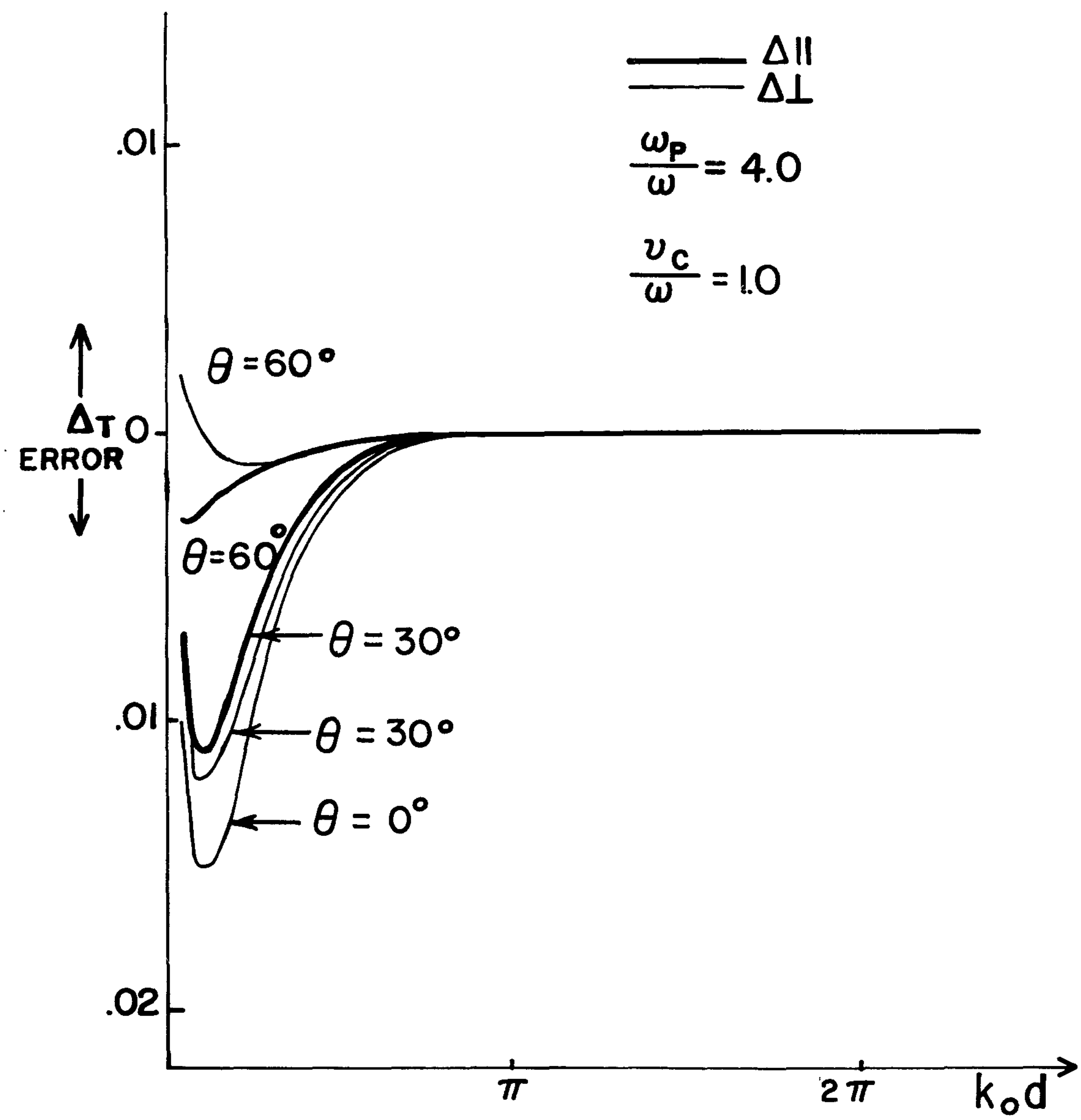

Fig. 9b. First Approximation Transmission Error ($\omega_p/\omega = 4$)

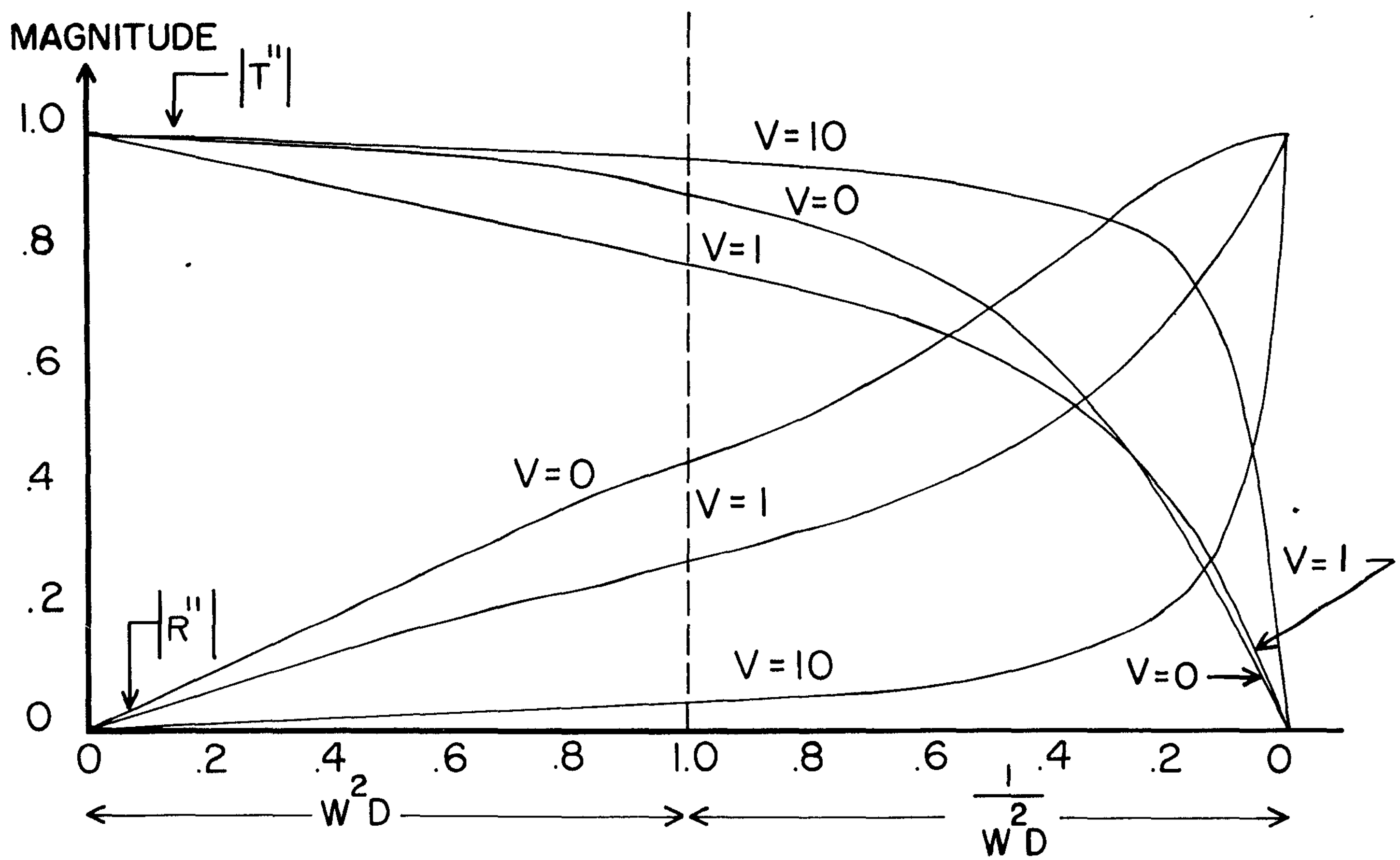

Fig. 10a. Jump Solution (Magnitude)

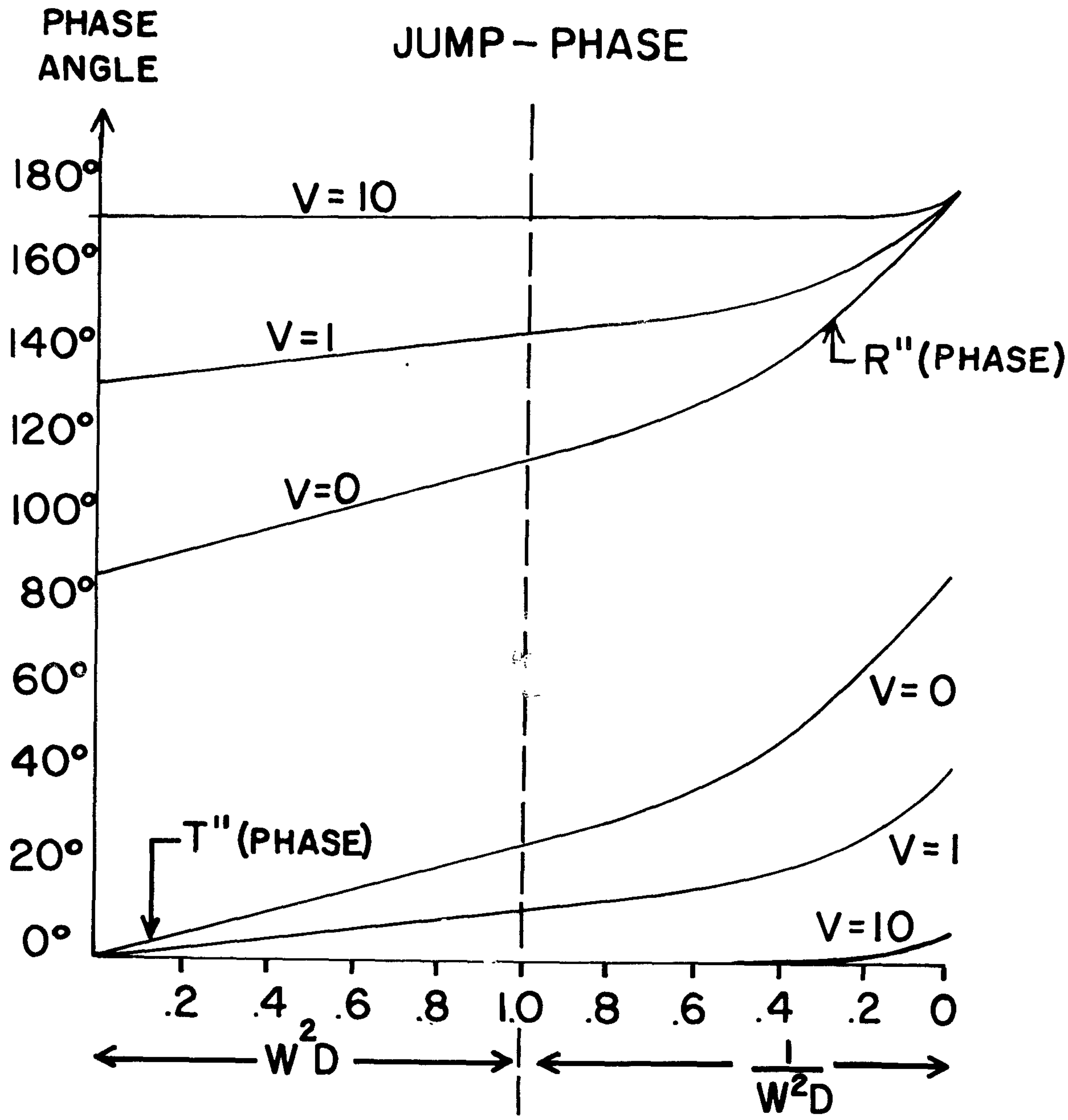

Fig. 10b. Jump Solution (Phase)

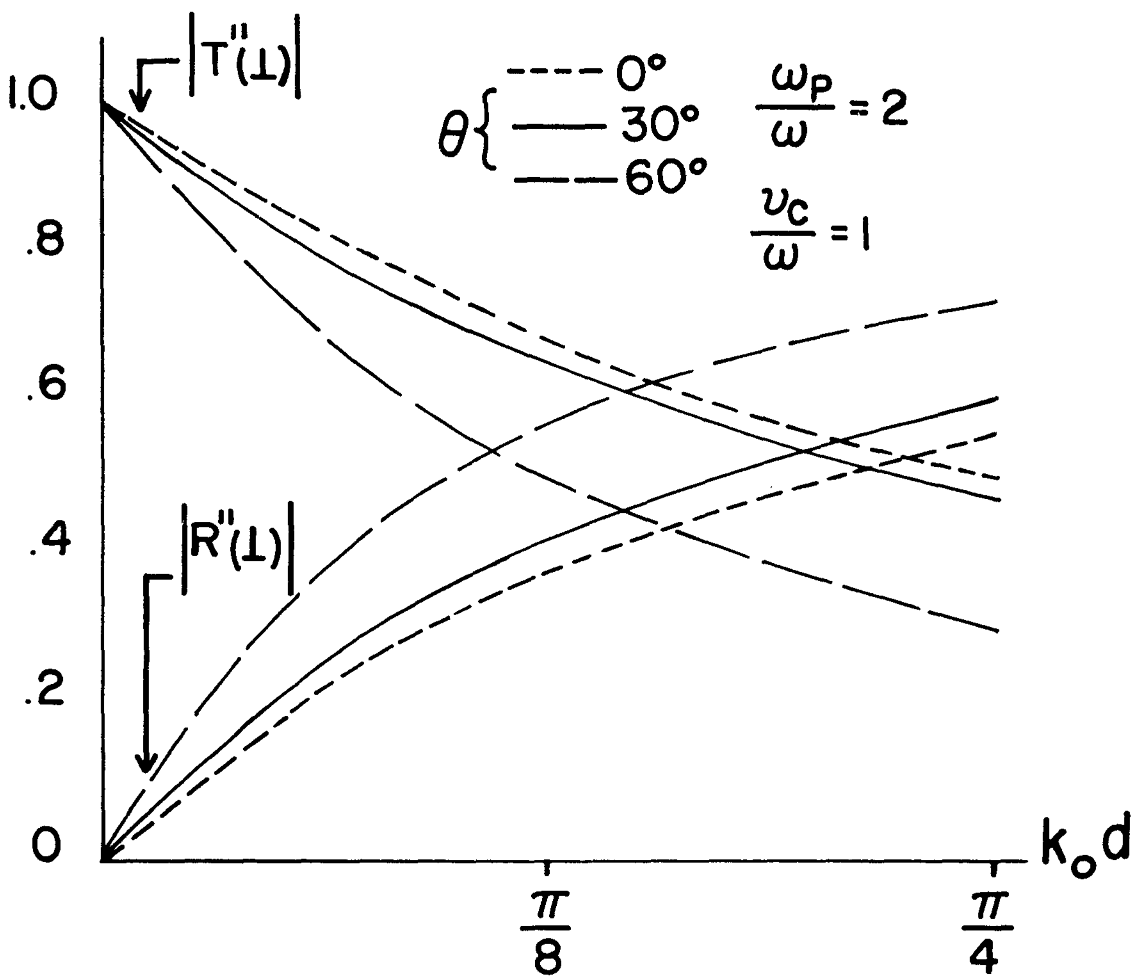

Fig. 11a. Second Approximation, Lossy, $\omega_p/\omega = 2$ (TE Mode)

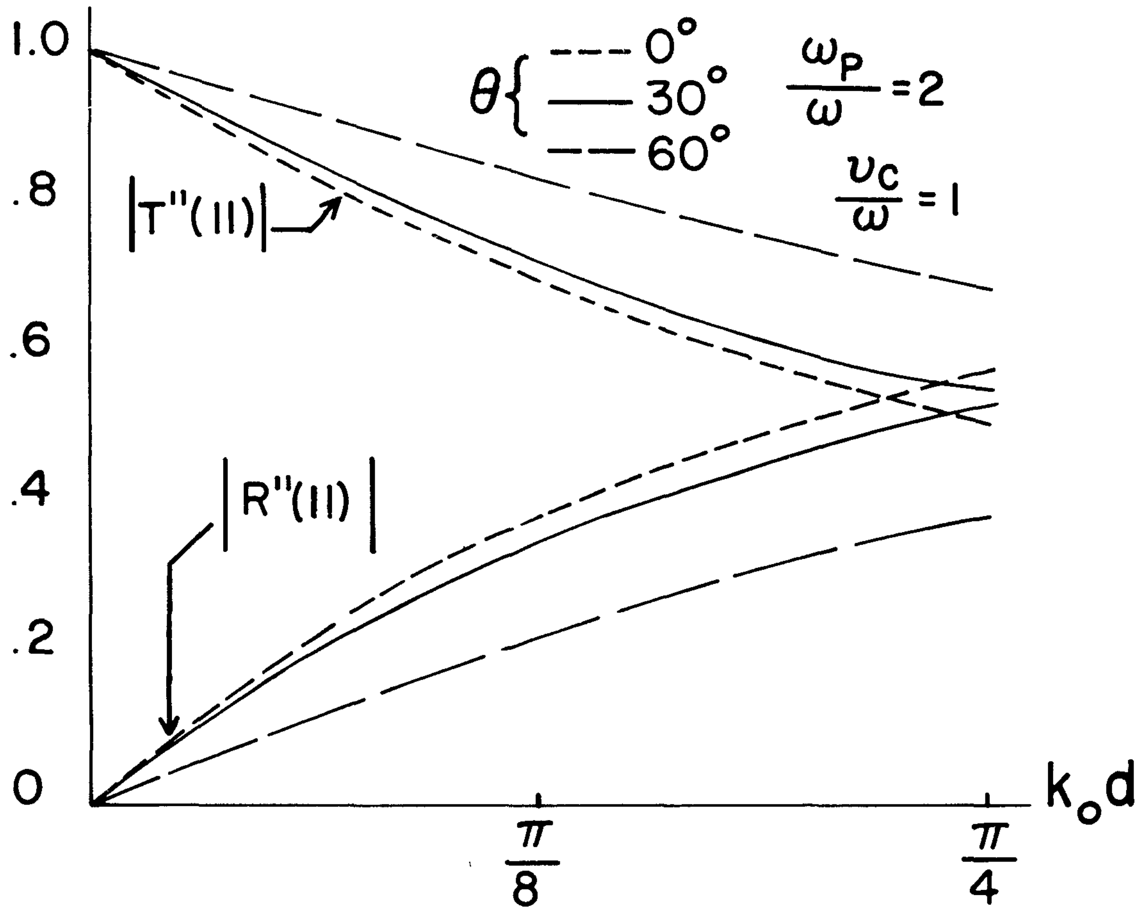

Fig. 11b. Second Approximation, Lossy, $\omega_p/\omega = 2$ (TM Mode)

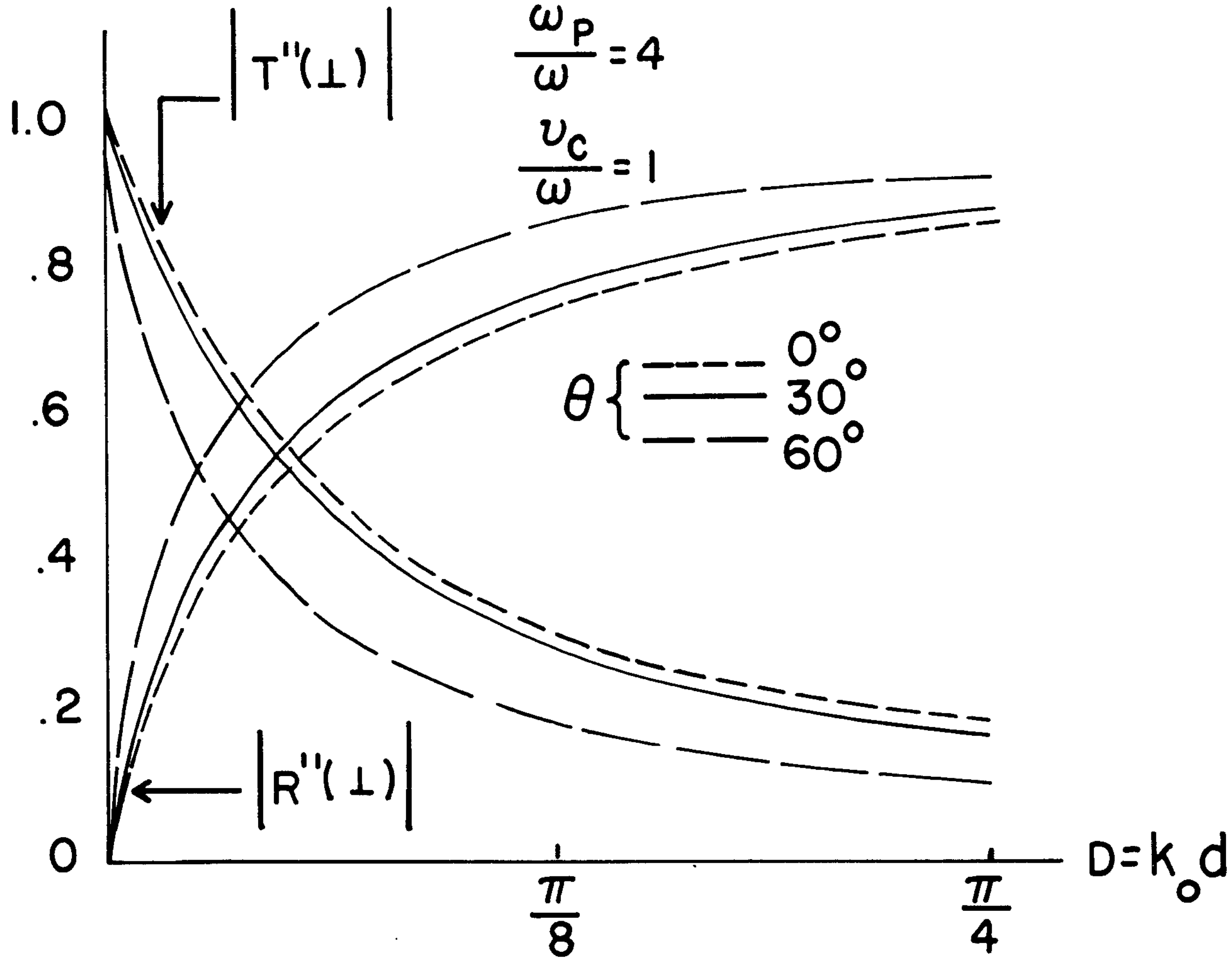

Fig. 12a. Second Approximation, Lossy, $\omega_p/\omega = 4$ (TE Mode)

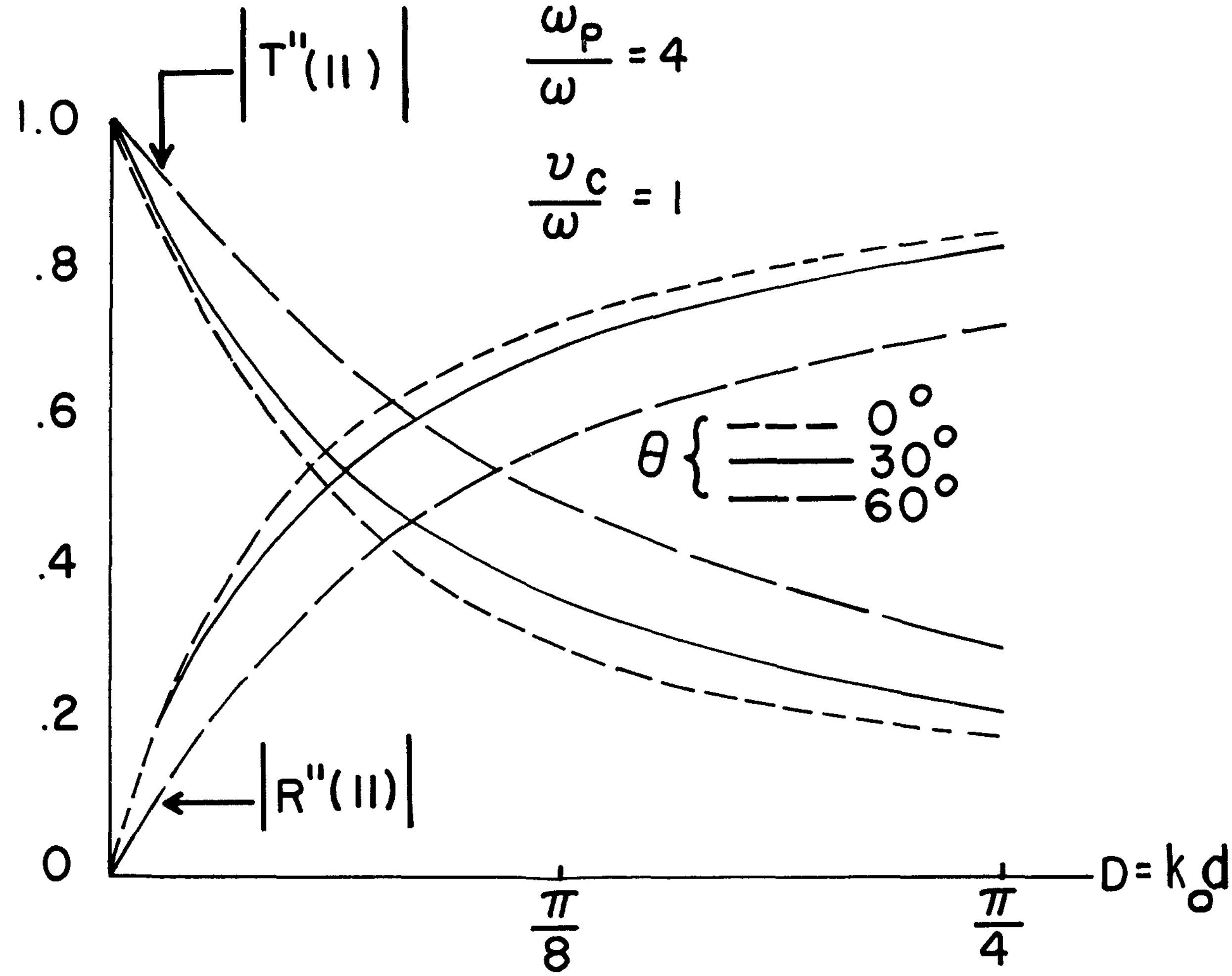

Fig. 12b. Second Approximation, Lossy, $\omega_p/\omega = 4$ (TM Mode)

REFERENCES

1. W. Rotman, "Plasma Simulation by Artificial Dielectric and Parallel-Plate Media," I.R.E. Trans. on Antennas and Propagation, Vol. AP10 No. 1, 82-95, (January 1962).

2. J. Brown, "Artificial Dielectrics Having Refractive Indices Less than Unity," Proc. I.E.E., Monograph No. 62R, Vol. 100, Part 4, 51-62 (May 1953).

3. G. G. McFarlane, "Surface Impedance of an Infinite Parallel-Wire Grid at Oblique Angles of Incidence," Journal I.E.E., (London), Part IIIA, 93, 1923-1527 (1947).

4. J. K. Skwirzynski and J. C. Thackray, "Transmission of Electromagnetic Waves Through Wire Gratings (Theory)," Marconi Review, 22, Second Quarter, 77-90 (1959).

5. K. E. Golden and T. M. Smith, "Simulation of a Thin Plasma Sheath by a Plane of Wires," to be published I.E.E.E. Transactions on Nucl. Sci., Vol. NS11 No. 1 (January 1964).

6. E. C. Taylor, "Approximate Boundary Conditions for Plasma Sheaths," to be published, Aerospace Corporation, El Segundo, Calif.

7. E. C. Jordan, "Electromagnetic Waves and Radiating Systems," (Prentice-Hall, Inc., New York, N.Y., pp. 143-147 and 155-158, 1950).

8. J. R. Wait, "The Electromagnetic Fields of a Dipole in the Presence of a Thin Plasma Sheet," Appl. Sci. Res., 8, Section B, 397-417 (1960).

9. R. H. Gold, "Reflection and Transmission of Electromagnetic Waves from Inhomogeneous Magnetoactive Plasma Slabs," TDR-169(3230-11)TN-12 No.(AF 04(695)-169), Aerospace Corp., El Segundo, Calif., p. 22 (March 1963).

10. R. G. Jahn, "Interaction of Electromagnetic Waves and Slightly Ionized Gases," Calif. Inst. of Tech., Tech. Note No. 2, p. 15, Pasadena, Calif., Af 49(638)-758, (August 1960).

DISTRIBUTION

Internal

Aseltine, J. A.
Barlow, E. J.
Batdorf, S. B.
Becker, R. A.
Billings, B. H.
Griesser, W. A.
Getting, I. A.
Hartunian, R. A.
Hlavka, G. E.
Logan, J. G.
Mager, A.
Mirels, H.
Moss, B.
Payne, R. E.
Pearce, K.
Targoff, W. P.
Weiss, M. T.
Hove, J. E.
Betchov, R.
Bleviss, Z. O.
Caron, P. R.
Comisar, G. G.
Dazey, M. H.
Dix, D. M.
Eastmond, E. J.
Fuhs, A. E.
Golden, K. E.
Grewal, M. S.
Huddlestone, R. H.
Kolpin, M. A.
Leonard, S. L.
Light, G. C.
Lu, A. Y.
McPherson, D. A.
Meyer, R. X.
Pridmore-Brown, D. C.
Stewart, G. E.
Taylor, E. C.
Turner, E. B.
Wood, J. G.

External

Defense Documentation Center
(DDC) 20 copies
Cameron Station
Alexandria, Virginia

SSD (SSTRE/Maj. Lewis, Jr.)

AFCRL (ERD Library)
L. G. Hanscom Field
Bedford, Mass.

AFCRL (CRRB)
L. G. Hanscom Field
Bedford, Mass.

DISTRIBUTION (Continued)

External (Continued)

AFOSR (Library)
Bldg. T-D
Washington 25, D. C.

HQ DDC
Bldg. 5
Cameron Station
Alexandria, Virginia

AFWL (Library)
Kirtland AFB
New Mexico

Library of Congress
Washington 25, D. C.

NASA (Library)
Ames Research Center
Moffett Fld, Calif.

HQ NASA
400 Maryland Ave. SW
Washington 25, D. C.

NASA (Library)
Langley AFB, Va.

AVCO
Wilmington, Massachusetts
ATTN: M. C. Adams

AVCO Everett Research Laboratory
2385 Revere Beach Parkway
Everett 49, Mass.
ATTN: A. Kantrowitz

AVCO Everett Research Laboratory
2385 Revere Beach Parkway
Everett, Mass.
ATTN: H. E. Petschek

Aeronutronic Division of Ford Motors Corp.
Ford Road
Newport Beach, Calif.
ATTN: S. R. Byron

Bell Telephone Laboratory
Murray Hill, N. J.
ATTN: S. Buchsbaum

Boeing Scientific Research Laboratory
Seattle, Washington
ATTN: J. E. Drummond

Brooklyn Polytechnic Institute
Brooklyn 1, New York
ATTN: A. Ferri

Brooklyn Polytechnic Institute
Brooklyn 1, New York
ATTN: N. Markowitz

California Institute of Technology
1201 E. California
Pasadena, California
ATTN: J. D. Cole

NASA (Library)
Lewis Research Center
21000 Brookpark Road
Cleveland 35, Ohio

NASA (Library)
Marshall Space Flight Center
Huntsville, Alabama

National Bureau of Standards (Library)
Washington 25, D. C.

External (Continued)

AF Cambridge Research Lab.
Missile Antenna Branch
Office of Aerospace Research
Hanscom Field, Mass.
ATTN: W. Rotman

National Bureau of Standards
Boulder, Colorado
ATTN: J. R. Wait

AF Avionics Laboratory
R&T Division
Wright-Patterson AFB, Ohio

NASA (V. J. Rossow)
Ames Research Center
Moffett Field, Calif.

NASA (A. Busemann)
Langley AFB, Va.

NASA (W. Moeckel)
Lewis Research Center
21000 Brookpark Road
Cleveland 35, Ohio

General Electric Co.
Knolls Research Laboratory
P. O. Box 1088
Schnectady, New York
ATTN: H. Hurwitz

General Electric Co.
MAVD, Valley Forge
Philadelphia, Pennsylvania
ATTN: L. Steg

High Altitude Observatory
Boulder, Colorado
ATTN: S. Chapman

Hughes Research Laboratory
Malibu, Calif.
ATTN: R. C. Knechtli

I. I. T. Research Institute
10 W. 35th Street
Chicago, Illinois
ATTN: S. W. Kash

Johns Hopkins University
Department of Aeronautics
Baltimore 18, Maryland
ATTN: F. H. Clauser

Lockheed Missiles and Space Center
Sunnyvale, California
ATTN: R. Landshoff

Los Alamos Scientific Laboratory
P. O. Box 1663
Los Alamos, New Mexico
ATTN: J. M. B. Kellog

Los Alamos Scientific Laboratory
Los Alamos, New Mexico
ATTN: C. L. Longmire

Massachusetts Institute of Technology
Cambridge 39, Mass.
ATTN: E. E. Covert

Massachusetts Institute of Technology
Cambridge 39, Mass.
ATTN: D. J. Rose

Massachusetts Institute of Technology
Dept. of Mechanical Engineering
Cambridge 39, Mass.
ATTN: J. L. Kerrebrock

DISTRIBUTION (Continued)

External (Continued)

Naval Ordnance Lab. (Tech. Library)
White Oaks
Silver Springs 19, Maryland

Naval Research Lab.
Director, Tech. Info. Officer
Code 2000
Washington 25, D. C.

Oak Ridge National Lab (Library)
P. O. Box Y
Oak Ridge, Tennessee

Office of Tech Services
Tech. Reports Section
Dept. of Commerce
Washington 25, D. C.

ONR Branch
Commanding Officer
1030 Green Street East
Pasadena, Calif.

RADC (Library)
Griffis AFB, N. Y.

US Army Signal R&D Lab (Data Equip. Br.)
Technical Info. Officer
Fort Monmouth, New Jersey

California Inst. of Technology
1201 E. California Street
Pasadena, California
ATTN: R. W. Gould

California Institute of Technology
1201 E. California Street
Pasadena, California
ATTN: L. Lees

California Institute of Technology
1201 E. California Street
Pasadena, California
ATTN: Library

California Institute of Technology
1201 E. California Street
Pasadena, California
ATTN: W. H. Liepmann

General Atomics
La Jolla, California
ATTN: R. H. Lovberg

General Atomics
La Jolla, California
ATTN: N. Rostoker

General Electric Co.
Knolls Research Laboratory
P. O. Box 1088
Schnectady, New York
ATTN: R. Alpher

US Atomic Energy Commission
(Dir of Research)
Washington 25, D. C.

US Atomic Energy Commission
Tech Info. Service Extension
P. O. Box 62
Oak Ridge, Tennessee
US Naval Research Lab. (Library)
Washington, D. C.

Wright Air Development Center
(Library)
Wright-Patterson AFB, Ohio

SSTP - Capt. D. De Bus 3/205C

DISTRIBUTION (Continued)

External (Continued)

Massachusetts Institute of Technology
Research Laboratory of Electronics
Cambridge 39, Mass.
ATTN: S. C. Brown

NASA Ames Research Center
Moffett Field, Calif.
ATTN: V. J. Rossow

NASA Langley Field Research Center
Langley, Virginia
ATTN: A. Busemann

NASA Lewis Research Center
21000 Brookpark Road
Cleveland 35, Ohio
ATTN: W. Moeckel

NASA Marshall Space Flight Center
Huntsville, Alabama
ATTN: E. Stuhlinger

New York University
Institute of Mathematical Sciences
25 Waverly Place
New York 3, New York
ATTN: H. Grad

Northwestern University
Department of Physics
Evanston, Illinois
ATTN: R. Hines

Northwestern University
Evanston, Illinois
ATTN: A. B. Cambel

Princeton University
Physics Department
Princeton, New Jersey
ATTN: E. A. Frieman

Princeton University
Physics Department
Princeton, New Jersey
ATTN: T. H. Stix

Princeton University
Project Matterhorn
Princeton, New Jersey
ATTN: M. B. Gottlieb

Rand Corporation
1700 Main Street
Santa Monica, California
ATTN: C. Gazley, Jr.

Space Technology Laboratories, Inc.
1 Space Park
Redondo Beach, Calif.
ATTN: S. Alshuler

Space Technology Laboratories, Inc.
1 Space Park
Redondo Beach, California
ATTN: D. Langmuir

Stanford University
Stanford, California
ATTN: D. Bershader

Stanford University
Stanford, California
ATTN: O. Buneman

Stevens Institute of Technology
Department of Physics
Hoboken, New York
ATTN: George Schmit

Stanford University
Stanford, California
ATTN: P. Sturrock

DISTRIBUTION (Continued)

External (Continued)

University of California
Berkeley, California
ATTN: A. Trivelpiece

University of California
Physics Department
Berkeley, California
ATTN: A. Kaufmann

University of California
Physics Department
Berkeley, California
ATTN: W. B. Kunkel

University of California
Lawrence Radiation Laboratory
Berkeley, California
ATTN: J. M. Wilcox

University of California
Lawrence Radiation Laboratory
P. O. Box 808
Livermore, California
ATTN: W. Heckrotte

University of California
Lawrence Radiation Laboratory
P. O. Box 808
Livermore, California
ATTN: C. Van Atta

University of California
Physics Department
Los Angeles 24, Calif.
ATTN: A. Baños, Jr.

University of California
Physics Department
Los Angeles, Calif.
ATTN: B. D. Fried

University of California
School of Engineering
Los Angeles 24, Calif.
ATTN: N. Rott

University of Chicago
Enrico Fermi Institute for Nuclear Studies
Chicago 37, Illinois
ATTN: S. K. Allison

University of Colorado
Physics Dept.
Boulder, Colorado
ATTN: W. E. Brittin

University of Illinois
Department of Electrical Engineering
Urbana, Illinois
ATTN: Paul D. Coleman

University of Illinois
Physics Department
Urbana, Illinois
ATTN: D. Jackson

University of Maryland
College Park, Maryland
ATTN: J. M. Burgers

University of Maryland
College Park, Maryland
ATTN: S. I. Pai

University of Michigan
Ann Arbor, Michigan
ATTN: O. Laporte

External (Continued)

University of Minnesota
Physics Department
Minneapolis, Minnesota
ATTN: P. Kellog

University of North Carolina
Physics Department
Chapel Hill, North Carolina
ATTN: W. H. Bennett

University of Southern California
Los Angeles 7, California
ATTN: A. Kaprelian

University of Southern California
Los Angeles 7, Calif.
ATTN: T. Koga

University of Tennessee
Department of Physics and
Astronomy
Knoxville, Tennessee
ATTN: E. G. Harris

US Naval Research Laboratory
Washington, D. C.
ATTN: A. C. Kolb

Westinghouse Research Laboratories
Beulah Road,
Pittsburgh 35, Penn.
ATTN: R. E. Fox

Electro Optical Systems, Inc.
125 No. Vinedo
Pasadena, California
ATTN: A. T. Forrester

Marquette University
1515 West Wisconsin Ave.
Milwaukee 3, Wisconsin
ATTN: J. D. Horgan

Marquette University
1515 West Wisconsin Ave.
Milwaukee 3, Wisconsin
ATTN: T. K. Ishii

Syracuse University
Dept. of Electrical Engineering
Syracuse, New York
ATTN: R. F. Harrington

Johns Hopkins University
Baltimore 18, Maryland
ATTN: L. S. G. Kovasznay

Boeing Company
Physics Technology Dept.
P. O. Box 3707
Seattle 24, Washington
ATTN: J. S. Yee